Chemostratigraphy of Cambrian Carbonates from the Amadeus Basin: Implications for Paleo-Depositional Environments and Marine Redox

Thesis submitted in accordance with the requirements of the University of Adelaide for an Honours Degree in Geology

Qudsiya Hamed Al-Busaidi

November 2018

THE UNIVERSITY of ADELAIDE

CHEMOSTRATIGRAPHY OF CAMBRIAN CARBONATES IN THE AMADEUS BASIN: IMPLICATIONS FOR PALEO-DEPOSITIONAL ENVIRONMENTS AND MARINE REDOX.

RUNNING TITLE

Chemostratigraphy of Cambrian Carbonates in the Amadeus Basin

ABSTRACT

The Paleozoic sedimentary sequences from the Amadeus Basin in the Northern Territory (NT) have been a subject of several studies due to their economic and scientific significance. However, the applications of trace element and/or stable and radiogenic isotope proxies (e.g., REE, C and Sr isotopes) to Cambrian carbonate records from the Amadues Basin are quite limited. Strontium isotope ratio ($^{87}Sr/^{86}Sr$) and the major and trace elemental concentration data (including REE, and paleo-redox Ce anomaly) were used in this study to constrain the paleo-depositional environment and the redox conditions in the NE parts of the Amadeus Basin during the middle Cambrian, based on analysis of carbonates from two drill cores (Alice 1 and Dingo2). Importantly, acquired data from these two remote cores are consistent with a presumably regional and perhaps basin-wide signal. In detail, this study shows that the lower or older successions (Giles Creek Dolomite mainly) have $^{87}Sr/^{86}Sr$ record that is consistent with the expected coeval middle Cambrian paleo-seawater Sr isotope composition, and REE data point to more oxic conditions. This in turn suggests either a limited restriction of the basin from the Cambrian global ocean during this time (~515 to 505 Ma), or alternatively an existence of "evaporitic seaway" settings. Considering the evidence for major evaportic cycles in the studied records, the latter scenario is more plausible. In contrast, the upper and younger successions have $^{87}Sr/^{86}Sr$ ratio that is non-marine and much more radiogenic, plus REE data indicate more reducing conditions. These proxy data thus indicate a substantial restriction of the basin during this time (~505 to 495 Ma) and an overall increase in the input of continental Sr flux into the basin via weathering, likely due to more humid climate. Overall, this study argues that the older middle Cambrian sedimentary record from the Amadeus Basin was deposited under generally oxic conditions while still being connected at some level to the open ocean during times of hotter or greenhouse climate, the latter reflected as repetitive evaporitic cycles. The younger Cambrian record, during the positive C isotope (SPICE) event, was in contrast deposited under more reducing redox conditions and enhanced continent-derived weathering fluxes, driven by climate change (arid to humid), amplified by the equatorial position of the Amadeus Basin during the Cambrian times.

KEYWORDS

Chemostratigraphy, Amadeus Basin, Strontium Isotopes, Rare Earth Elements, Basin Restriction, Redox, Depositional Environment

TABLE OF CONTENTS

Chemostratigraphy of cambrian carbonates in the amadeus basin: implications for paleo-depositional environments and marine redox. i
Running title i
Abstract i
Keywords i
List of Figures and Tables 1
1. Introduction 2
2. Geological Setting/Background 5
3. Methods 8
3.1 Sample Selection 8
3.2 Sample Preparation: Sequential Leaching 8
3.3 Element Analysis 9
Major and Trace Elements Concentration Analysis 9
Rare Earth Elements (REE) 9
3.4 Radiogenic Strontium ($^{87}Sr/^{86}Sr$) Isotope Analysis 10
Chromatographic Purification of Strontium 10
TIMS Analysis of $^{87}Sr/^{86}Sr$ 10
Correction of $^{87}Sr/^{86}Sr$ for In-Situ Decay of ^{87}Rb 11
4. Results 11
4.1 Element Analysis 11
Major and Trace Elements 11
Rare Earth Elements (REE) 13
4.2 $^{87}Sr/^{86}Sr$ Isotope Analysis 15
5. Discussion 17
5.1 Evaluation of Diagenesis and Clay Contamination on the Primary Isotope Signals in Cambrian Marine Carbonates 17
5.2 Paleo-Redox Proxies in Marine Settings 19
5.3 Sr Isotope Constraints on Paleo-Depositional Environment 21
Evaporitic Cycles and Constraints on the Restriction of the Basin 22
The Steptoean Positive Carbon Isotope Excursion (SPICE) 24
5.4 Correlation with $^{87}Sr/^{86}Sr$ Global Curve 27
6. Conclusions 28
Acknowledgments 29
References 31

Appendix A: Extended Methods 34
Appendix B: Calculations..... 35
Appendix C: Full Data Set..... 36

LIST OF FIGURES AND TABLES

Figure 1 Stable carbon isotope ($\delta^{13}C$) record of Amadeus Cambrian carbonates from .. 4
Figure 2 a) Map of Australian Cambrian-Ordovician basins and interpreted depositional environments. b) Stratigraphy of Amadeus basin (Schmid, 2017). c) Map of the Amadeus basin..... 7
Figure 3 Elemental concentrations versus stratigraphic depth 13
Figure 4. Ce and Pr anomaly data (Ce/Ce* and Pr/Pr*) versus stratigraphic depth..... 14
Figure 5. Sr and C isotopic trends and Sr/Ca ratio versus depth 16
Figure 6. Cross plot of elemental concentrations versus Sr isotope signatures..... 18
Figure 7. Cross-plot of shale-normalized (PAAS) Ce/Ce* and Pr/Pr* anomalies 21
Figure 8. Global paleo-geography map of the Cambrian period (514 Ma) 24
Figure 9. Sr isotopic ratio and Ce anomaly versus $\delta^{13}C$ during the SPICE anomaly..... 27
Figure 10. The $^{87}Sr/^{86}Sr$ record of published sources and this study during the middle to upper Cambrian (~510 to ~485 Ma)..... 28

1. INTRODUCTION

The intracratonic Amadeus Basin located in the Northern Territory of Australia has been explored by many geological and geophysical studies, through research collaborations between the industry, universities and the Northern Territory Geological Survey (NTGS) due to its high scientific and economical significance. Economically, it hosts commercial hydrocarbon fields, with the potential of hosting further undiscovered resources, including conventional and unconventional petroleum (Ahmad & Munson 2013; Jarrett, Edwards, Boreham, & McKirdy, 2016; Marshall, 2005; Munson, 2014). Scientifically, it provide us with a unique window into the evolution of the Earth's system covering a period of ca. 500 million years (Ma), as it contains one of the world's best exposed and preserved archives of Neoproterozoic to ealry Palaeozoic sedimentary rocks (Kennard & Korsch, 2017). These also include sequences of Cambrian shallow-marine carbonates, which thus represent valuable records of geological and biological evolution during this critical time in the Earth's history. The Cambrian period was associated with a major biological event known as 'The Cambrian Explosion', as well as several environmental and climatic changes, which are reflected in changes in the isotope composition of the Cambrian oceans, that were recorded in marine carbonates. For example, carbon isotope variations ($\delta^{13}C$) in marine carbonates can be used to infer past changes in the marine carbon cycle and biological productivity in the oceans, whereas radiogenic strontium isotopes ($^{87}Sr/^{86}Sr$) provide information on tectonic history of our planet (e.g. weathering vs. hydrothermal processes). In addition, the $^{87}Sr/^{86}Sr$ composition of well-preserved marine carbonates can be also used to date and correlate sedimentary sequences worldwide (i.e., Strontium Isotope Stratigraphy), which is based on the fact the $^{87}Sr/^{86}Sr$ ratio in the ocean water is globally homogenous

and has varies through geological time (McArthur, Howarth, & Shields, 2012; Zhao, Zheng, & Chen, 2009). Thus far, the potential of Strontium Isotope Stratigraphy to date and correlate carbonates deposited in the Amadeus Basin has not been fully explored.

The early Paleozoic deposits in the Amadeus Basin consists of sedimentary successions, including shallow-water marine and subtidal carbonates of Middle to Late Cambrian age (Schmid, 2017). Schmid (2017) suggested that the lower Cambrian successions of the Amadeus basin were deposited under shallow oxygenated waters that change progressively towards more anoxic marine environments up the stratigraphy. Furthermore, Schmid (2017) identified a 2nd order and multiple 3rd order cyclicity in Cambrian sedimentary sequences within the basin, that were interpreted as repetitive evaporitic cycles similar to the evaporitic Permian Zechstein cycles, and the above study was also able to successfully correlate these cycles with the record of global sea level cycles published by Babcock et al. (2015). Moreover, a complete record of $\delta^{13}C$ variations in the Cambrian carbonates from the Amadeus Basin was published recently by Schmid (2017) where the three major and global Cambrian C-isotope excursions were identified and documented from multiple drill cores, including: SPICE (Steptoean Positive Carbon Isotope Excursion), DICE (Drumian Carbon Isotope Excursion) and ROECE (Redlichiid-Olenellid Extinction carbon Isotope Excursion), which all seem to be associated with conditions of highstand system tract (Schmid, 2017).

The primary objective of this study is to generate the first continuous carbonate $^{87}Sr/^{86}Sr$ record for the Amadeus Basin during the Cambrian period, and using it as a tool to (i) understand changes in paleo-depositional environments, (ii) reconstruct possible restriction events of the Amadeus basin relative to the Cambrian open ocean, and (iii) to correlate carbonate units using global/local Sr isotope stratigraphy approach. In addition, this study also aims to reconstruct paleo-redox conditions in the basin

during the deposition of Cambrian carbonates. This will be done via analysis of rare earth elements (REE) in selected carbonates, and specifically using cerium anomaly (Ce/Ce*) as a proxy for paleo-redox conditions in marine environments (Tostevin et al., 2016). Finally, using a multi-proxy approach based on Sr isotopes and REE, this study also aims to understand changes in marine paleo-environment and redox conditions that have led to the formation of (i) local evaporitic cycles, and (ii) globally recognised and prominent SPICE carbon isotope anomaly, whose origin is controversial and hotly debated topic (Schmid, 2017, and references therein).

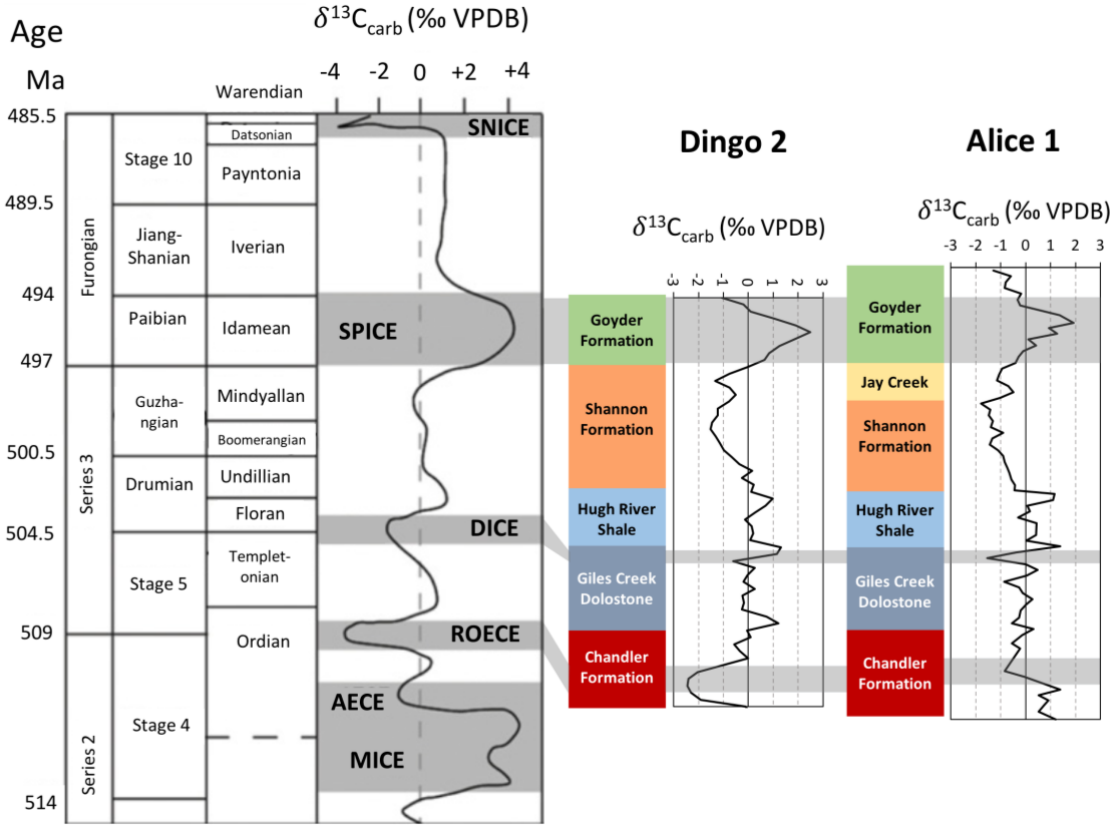

Figure 1 Stable carbon isotope ($\delta^{13}C$) record of Cambrian carbonates from Amadeus Basin from Schmid (2017), based on analysis of carbonated from Dingo 2 and Alice 1 cores, correlated with the global carbon isotope curve (i.e., Left Diagram, data from: Peng, Babcock, & Cooper, 2012).

2. GEOLOGICAL SETTING/BACKGROUND

The Amadeus Basin is located South of the Northern Territory (NT) and extends 150 Km south into Central Australia, Covering a total area of about 170 000 Km^2. It contains Neoproterozoic to Early Carboniferous Stratigraphic successions reaching a maximum thickness of up to ~14 Km in some regions. The above sedimentary sequences overlie igneous and metamorphic basement rocks of the Precambrian Arunta region and Musgrave province. The Cambrian sedimentary record in the Amadeus Basin consists of pre-rift Early Cambrian dominated by fluvio-delatic to basinal deposits (Arumbera Sandstone) and post-rift Middle-Late Cambrian predominatly marine sediments. For the latter, the middle successions were deposited in a shallow marine, evaporitic oxic conditions (Chandler to lower Shannon Formations) while the late Cambrian sediments were dominated by non-hypersaline shallow marine conditions (Upper Shannon and Goyder Formation). The Amadeus Basin has different east to west successions of the Cambrian sedimentary rock records mainly due to varying depositional environments that ranges from shallow-marine to coastal and continental settings (see Figure 2).

The oldest Cambrian sedimentary rocks in the Amadeus Basin are the upper Arumbera Sandstones, which are conformably overlying the upper Proterozoic (Ediacaran) sedimentary rocks, specifically the Julie Formation carbonates (NE parts of the basin) or siliciclastic Inindia Beds (in SW parts of the Amadeus Basin). The stratigraphic age of the Arumbera Sandstone was constrained at Terreneuvian (~541 to 521 Ma) based on *Plagiogmus* trace fossils and other rare small shelly fossils, and it was deposited during the Petermann orogeny in deltaic-fluvial environments (Purdy, Cross, Brown, Carr, & Armstrong, 2016) with sediments sourced mostly from the south

from the Musgrave province (Schmid, 2017). The overlying Todd River Dolostone was assigned a Cambrian age of Series 2 Stage 3 (~521 to 517 Ma) based on biostratigraphy of Brachiopods, Archaeocyathids and correlations with nearby basins. The Todd River Dolostone Formation is limited to the eastern successions and marks the start of a marine transgression (Schmid, 2017), the latter recorded as a sequence of thinly bedded sandstones, siltstones and dolostones underlying a thickly bedded dolostone (ASUD, 2018). The stratigraphically younger and evaporitic Chandler Formation (Stage 4 to 5, ca. 515 to 506 Ma) is dominated by a thick salt units (mainly halite) that is only limited to the eastern successions and apart from evaporites this formation also contains carbonates (limestones/dolostones) extending to the central-west parts of the basin. The Chandler Formation was deposited under subaqueous and presumably anoxic conditions (Schmid, 2017). In NE parts of the basin, the overlying formation is the Giles Creek Dolostone that was dated at Stage 5 (~510 to 506 Ma) based on Trilobite species. This carbonate formation was deposited during sea level highstand on an open and generally shallow marine, subtidal carbonate platform (Schmid, 2017). The overlying Hugh River Shale composed of siltstone and shale units with few fine beds of dolostone and limestone is present mostly in the central parts of the Amadeus Basin, while in NE parts the time equivalent deposits are represented by carbonate-rich Shannon Formation (~506 to 497 Ma, Drumian and Guzhangian stages) deposited in the shallow marine environment during times of low sea level (Schmid, 2017). The Shannon Formation is classified as oolitic, Stramatolitic limestone deposited under intertidal to subtidal evaporitic conditions (Schmid, 2017). The upper Shannon formation is carbonate rich and was deposited during sea level rise, while the lower part of the formation is described as silty shale with interbedded dolostone, that was deposited in oxic, low energy, shallow marine environment (Schmid, 2017). The youngest Cambrian

formation investigated in this study is the Goyder Formation (~497 to 492 Ma, Paibian and Jiangshanian stages), covering the entire basin and represents the onset of major transgression and sea level rise that flooded nearshore siltstone and sandstone (Upper Goyder) and following the deposition of carbonates in shallow marine settings (Lower Goyder) (Schmid, 2017). Upper and Lower Goyder are separated by Hiatus. On the other hand, the western and more continentally dominated successions of the Amadeus Basin are characterized by lacustrine to fluvial depositional environments, this mainly reflects shallowing of the basin towards the west (see Figure 2A).

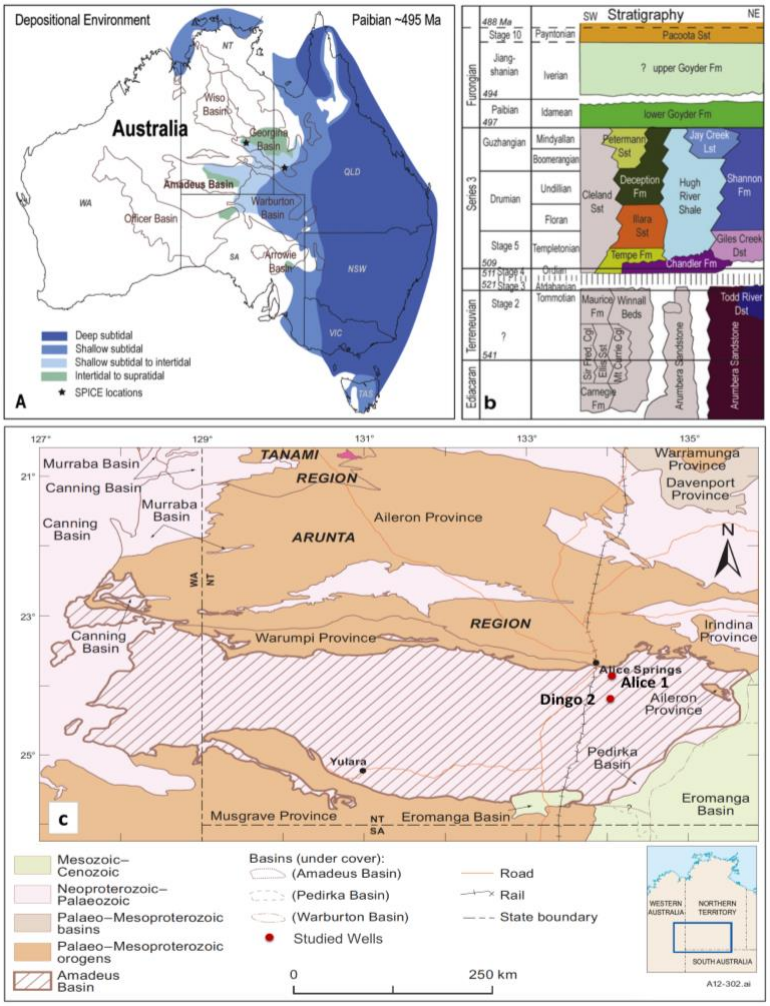

Figure 2 a) Map of Australian Cambrian-Ordovician basins and interpreted depositional environments during the upper Cambrian (Schmid, Smith, & Woltering, 2018). b) Stratigraphy of Amadeus basin (Schmid, 2017). c) Map of the Amadeus basin showing location of studied drill holes (Dingo 2 and Alice 1)

3. METHODS

3.1 Sample Selection

This study is based on a total of 86 bulk carbonate rock samples (i.e., powdered rock chips) collected from two petroleum drill cores, Dingo 2 and Alice 1, which are both located in the north-eastern part of the Amadeus Basin (Figure 2C). As the Cambrian depositional systems in Australia deepen towards the east, this part of the basin thus represents an ideal target sampling area where predominantly shallow to open marine environments preserved carbonate-rich records. The bulk carbonate samples for this study were collected with 10 to 50 meters resolution step, covering the Middle to Late Cambrian period (~520 to 495 Ma) with an overall thickness of about 1100 m. All samples analysed in this study were from NTGS archives, provided from the previous collection by Schmid (2017).

3.2 Sample Preparation: Sequential Leaching

Rock chips of 86 carbonate samples were crushed carefully into fine powder using Agate mortar and pestle, and homogenised carbonate powders were then weighted and sequentially leached (see below) to avoid possible clay contamination and to extract elements associated with carbonate phases. In detail, A 100 mg of powdered sample and/or standard (JDo-1 dolomite standard) were transferred into plastic centrifuge tubes, followed by 3-step-leaching procedure (modified from (Liu, Wang, & Raub, 2013). Firstly, powders were leached with 3.6ml of 1M ultra-pure ammonium acetate in Step 1 to liberate elements associated with exchangeable sites at clays (Edwards et al., 2015). Subsequently, 3.6ml of 0.2 ultra-pure acetic acid was used in Step 2 (acid leach was discarded), followed by Step 3 for 1 hour at room temperature to extract only elements

associated with carbonate phases (see Liu, Wang, & Raub, 2013). Between each step, all samples were sonicated for 30-40 minutes and then centrifuged at 3,600 rpm for 10 minutes before supernate were discarded in the first two steps and collected in the last step in small Teflon vials for elemental and isotopic analyses. The undissolved residue was dried and weighted to calculate the carbonate component leached and extracted from the original powder (Liu et al., 2013).

3.3 Element Analysis

MAJOR AND TRACE ELEMENTS CONCENTRATION ANALYSIS

The leachates from Step 3 were dried on a hotplate at 140℃ and then diluted with 2% Nitric acid into 1:1,700 aliquots for trace and rare earth elements (REE) analysis, and 1:100,000 aliquots were used for major elements analysis. Agilent 8900x (QQQ) Inductively Coupled Plasma Mass Spectrometer (ICP-MS) at Adelaide Microscopy centre was used to measure elemental concentration of 86 leached carbonate samples (including JDo-1 standard, and acid blanks).

RARE EARTH ELEMENTS (REE)

The shale-normalized Cerium anomaly (Ce/Ce*) can be used as a redox proxy due to different oxidation state of Ce (+3 and +4) relative to its neighbouring REE, such as Lanthanum (La) and Praseodymium (Pr) that both have only +3 valance or oxidation state (Tostevin et al., 2016). The Ce anomaly in this study was calculated based on the equation from (Taylor & McClennan, 1985), as follow:

$$Ce/Ce^{*} = [Ce/Ce_{(PAAS)}]/ [0.5 \times (La/La_{(PAAS)}) + 0.5 \times (Pr/Pr_{(PAAS)})] \quad \text{Eq.1}$$

Where PAAS stands for the 'Post-Archean Average Australian Shale' values.

In similar way, the Praseodymium (Pr/Pr*) anomaly was calculated relative to its neighbouring REE; Cerium and Neodymium (Nd), based on the equation from (Taylor & McClennan, 1985):

$$Pr/Pr^* = [Pr/Pr_{(PAAS)}]/[0.5 \times (Ce/Ce_{(PAAS)}) + 0.5 \times (Nd/Nd_{(PAAS)})] \quad \text{Eq.2}$$

3.4 Radiogenic Strontium ($^{87}Sr/^{86}Sr$) Isotope Analysis

CHROMATOGRAPHIC PURIFICATION OF STRONTIUM

Leached and dried samples (from Step 3) were redissolved in 1 ml of 8M Nitric Acid SD, and passed through Micro Bio-Spin columns filled with Sr specific resin (Eichrom Sr resin SPS) used to extract the pure Sr fraction from the sample matrix. The resins and columns were washed multiple times with 8M Nitric Acid and Ultra-pure denoised water before loading the samples and then the pure Sr fraction was collected using 0.05M Nitric Acid. A drop of 0.1M Nitric Acid was added to the collected Sr and procedural blanks were spiked at this point and were dried on a hotplate, following this, a squirt of 15M nitric acid was added to the samples to oxidise any organics (modified method from (Krabbenhöft et al., 2009).

TIMS ANALYSIS OF $^{87}SR/^{86}SR$

The purified Sr fractions were dried and loaded onto Rhenium filaments using Brick's Solution and Sr isotope abundances (i.e., $^{87}Sr/^{86}Sr$ ratios of carbonates) were measured in a multidynamic mode using ISOTOPX Phoenix Thermal Ionisation Mass Spectrometer (TIMS) in the University of Adelaide. Measurements are normalized to $^{86}Sr/^{88}Sr = 0.1194$, using exponential mass fractionation correction.

CORRECTION OF $^{87}SR/^{86}SR$ FOR IN-SITU DECAY OF ^{87}RB

In general, carbonate rocks tend to have low rubidium (Rb) and high strontium (Sr) content, however, the radiogenic Sr content may also increase over geological time due to decay of trace amounts of Rb present in the bulk carbonates, thus altering the primary marine or paleo-seawater $^{87}Sr/^{86}Sr$ isotopic signal recorded in ancient carbonates. The primary Sr isotopic composition was corrected using the following equation from (Nurgalieva, Ponomarchuk, & Nurgaliev, 2007):

$$(^{87}Sr/^{86}Sr)_0 = (^{87}Sr/^{86}Sr)_{Measured} - {}^{87}Rb/^{86}Sr \times (e^{\lambda t} - 1), \qquad \text{Eq.3}$$

Where λ is the ^{87}Rb decay constant of 1.42×10^{-11} yr^{-1} and t is the time in years, $(^{87}Sr/^{86}Sr)_{measured}$ is present-day isotope composition of carbonates, and $(^{87}Sr/^{86}Sr)_O$ is corrected composition for in-situ Rb decay. An average age (t) of 505 Ma was used to calculate the corrected $^{87}Sr/^{86}Sr$ ratios in this study and further discussion will be based on these corrected Sr isotope data.

4. RESULTS

4.1 Element Analysis

MAJOR AND TRACE ELEMENTS

All 86 carbonate samples analysed for their elemental concentration are shown in Figure 3, and plotted as a function of depth. Briefly, the Goyder Formation and the upper Shannon Formation contain the lowest Sr concentrations, as low as 31 ppm, while Sr concentrations in the lower Shannon Fm. spike to reach 618 ppm in Dingo 2 and 938 ppm in Alice 1, followed by two more Sr concentration spikes. The second spike occurring in the lower Giles Creek Formation reachs 1610 ppm in Dingo 2 and 4525

ppm in Alice 1. The third spike in Sr concentration appears only in Dingo 2 in the Chandler Formation as no samples were taken from this formation in Alice 1. Overall, the Sr concentration is systematically much higher in Alice 1 compared to Dingo 2, and our Sr concentrations trends generally agree with those published by Schmid (2017) analysed using a portable XRF device (see orange lines in Figure 3). The Sr/Mn ratio in marine carbonates is indicative of meteoric diagenesis (Banner and Hanson, 1990) where higher ratios (more Sr and less Mn) typically indicate little diagenetic overprint, and vice versa. Measured Sr/Mn is relatively low in the Goyder and the upper Shannon Formations and it generally increases down the stratigraphy to reach its highest values in the Giles Creek Dolostone (Sr/Mn ~5.6 in Dingo 2 and ~9.4 in Alice 1 cores). In addition, the Rb/Sr ratio of bulk marine carbonates can be used as an index for clay contamination and possible contribution of radiogenic ^{87}Sr from clay minerals (Paces, Peterman, Futa, Oliver, & Marshall, 2007). In Dingo 2, the Rb/Sr ratio is generally low with average of ~0.019 in the studied successions with the exception of the Goyder formation where it spikes to reach ~0.26. In Alice 1, the Rb/Sr ratio is relatively lower than in Dingo 2 with a maximum value of ~0.07 and a minimum value of ~0.0004, and with an average of ~0.012 (Figure 3). A complete list of all element concentrations measured in studied carbonates can be found in Appendix 1.

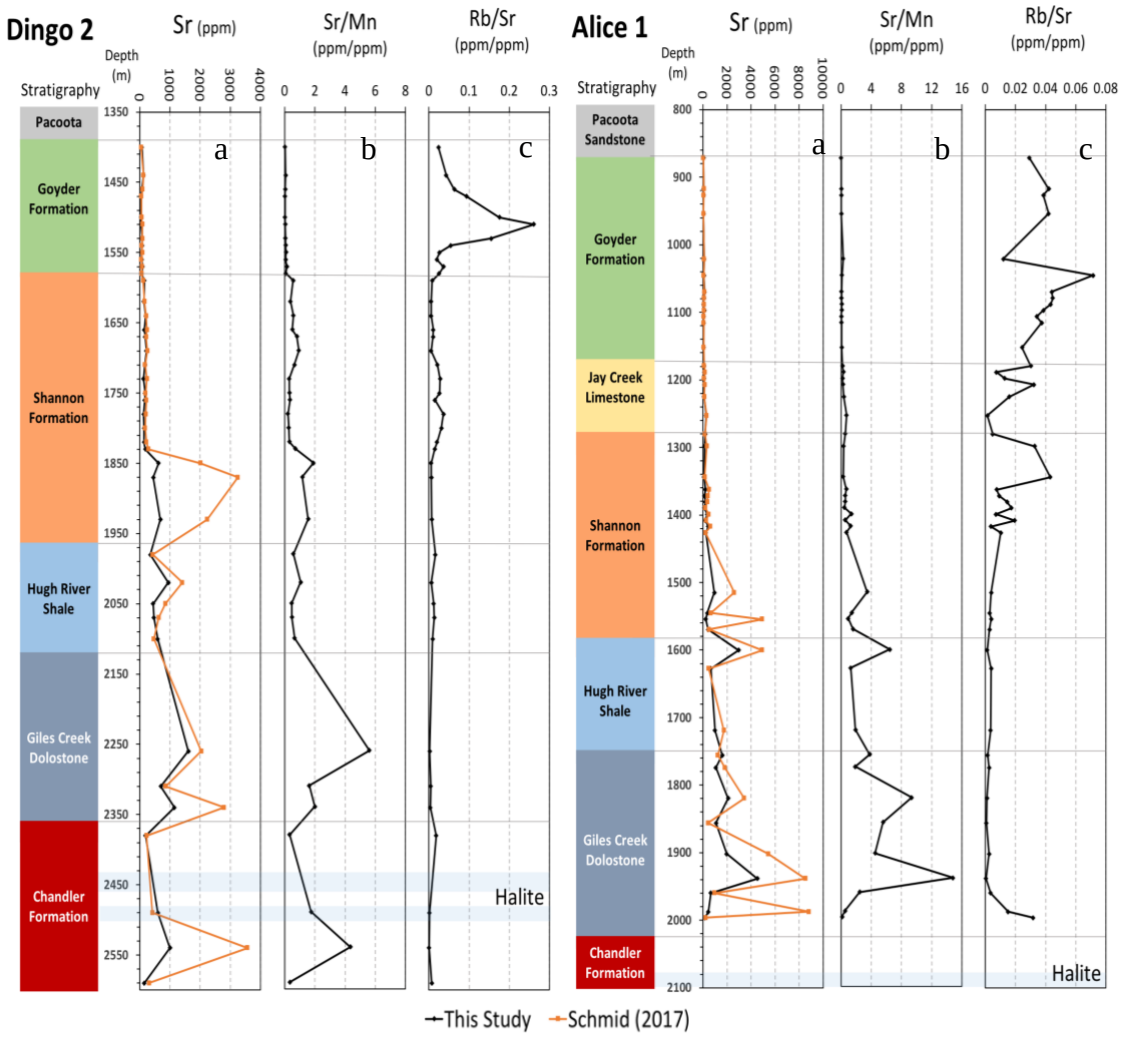

Figure 3 Elemental concentrations from Dingo 2 and Alice 1 versus stratigraphic depth. a) Sr concentration in ppm compared with data from Schmid (2017) (Black line: this study, Orange line: Schmid (2017)). b) Sr/Mn ratio to indicate diagenetic alteration. c) Rb/Sr ratio as an index for clay contamination.

RARE EARTH ELEMENTS (REE)

The concentration of rare earth elements (REE) in seawater and carbonates can be used as a valuable tool for understanding the paleo-redox conditions in ancient marine environments (de Baar, German, Elderfield, & van Gaans, 1988; G. Webb, Nothdurft, Kamber, Kloprogge, & Zhao, 2009). Cerium (Ce) and Praseodymium (Pr) anomalies are shown in Figure 4, plotted as a function of depth. Briefly, the Ce anomaly (Ce/Ce*) varies but generally becomes increasingly negative (indicating more oxic marine conditions) moving down the stratigraphy (Figure 4), with a maximum value of

~1.26 (positive anomaly) that is decreasing to ~0.66 (negative Ce anomaly) in Dingo 2. Similarly, Ce/Ce* decreases from a maximum of ~1.17 (positive anomaly) to ~0.88 (slight negative anomaly) in Alice 1 core. These data thus suggest generally more reducing conditions up the stratigraphy in both cores, and more oxic conditions recorded in the lower parts of the cores or stratigraphy. On the other hand, the Pr/Pr* anomaly is lowest in the Goyder Formation with values of ~0.87 and ~0.9 in Dingo 2 and Alice 1 respectively, and increases moving down the stratigraphy to reach a maximum of ~1.16 in the Chandler Formation in Dingo 2, and ~1.06 in Giles Creek Dolostone in Alice 1 (see Figure 4).

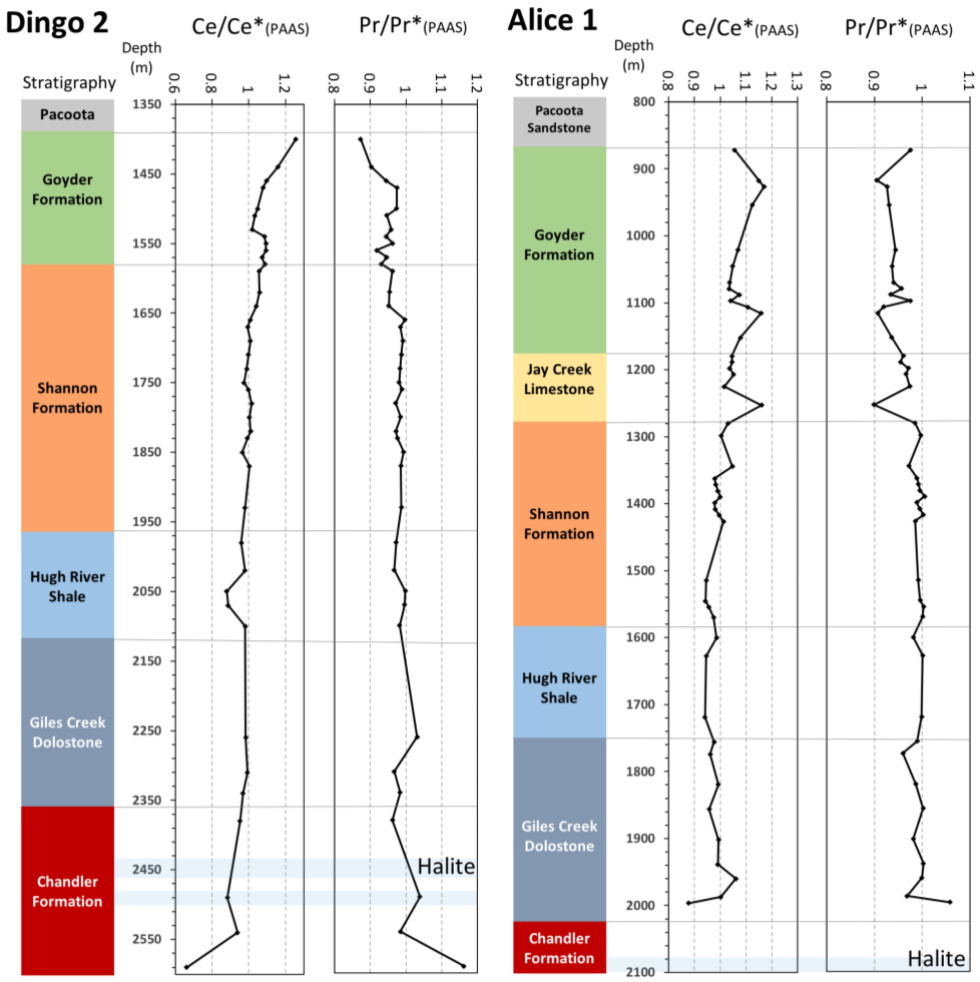

Figure 4. Ce and Pr anomaly data (Ce/Ce* and Pr/Pr*) calculated from measured REE concentrations in marine carbonates (using Eq. 1 and Eq.2 discussed in the methods), and plotted as a function of stratigraphic depth in Alice 1 and Dingo 2 cores.

4.2 $^{87}Sr/^{86}Sr$ Isotope Analysis

All samples analysed for their $^{87}Sr/^{86}Sr$ ratio are shown in Figure 5A, where the black line shows the measured $^{87}Sr/^{86}Sr$ values and the red line shows the $^{87}Sr/^{86}Sr$ values corrected for in-situ Rb decay using. In Dingo 2, corrected $^{87}Sr/^{86}Sr$ values varied from ~0.717502 to 0.709259 (2se=0.000004), and for Alice 1 the values ranged from ~0.713502 to ~0.709180 (2se=0.000004). The lowest or least radiogenic $^{87}Sr/^{86}Sr$ values occur in the Giles Creek Dolostone, some but not all data in this formation (from Alice 1) overlap with the expected Sr isotope composition of Cambrian seawater (0.7088 to 0.7093), as reconstructed for the studied interval by (McArthur et al., 2012; Montañez, Banner, Osleger, Borg, & Bosserman, 1996; Peng, Babcock, & Cooper, 2012). However, from Dingo 2, only one sample overlaps with expected paleo-seawater signature (see blue vertical rectangle in Figure 5A). The $\delta^{13}C$ record and data shown in Figure 5 was obtained from Schmid (2017) to illustrate the relationship between measured $^{87}Sr/^{86}Sr$ trends and the SPICE C-isotope anomaly. Results indicate that the $^{87}Sr/^{86}Sr$ record (both uncorrected and corrected for in-situ Rb decay) is most radiogenic in the Goyder Formation and appear to be closely linked with the coeval SPICE event and/or the largest positive $\delta^{13}C$ anomaly in the Cambrian. Furthermore, the Sr/Ca ratios are also plotted in Figure 5 to illustrate the position of evaporitic cycles identified in Alice 1 and Dingo 2 cores by Schmid (2017). The highly elevated Sr/Ca data point to two main evaporitic cycles observed in the sequences of Giles Creek Dolostone and the Shannon-Hugh River shales (Figure 5).

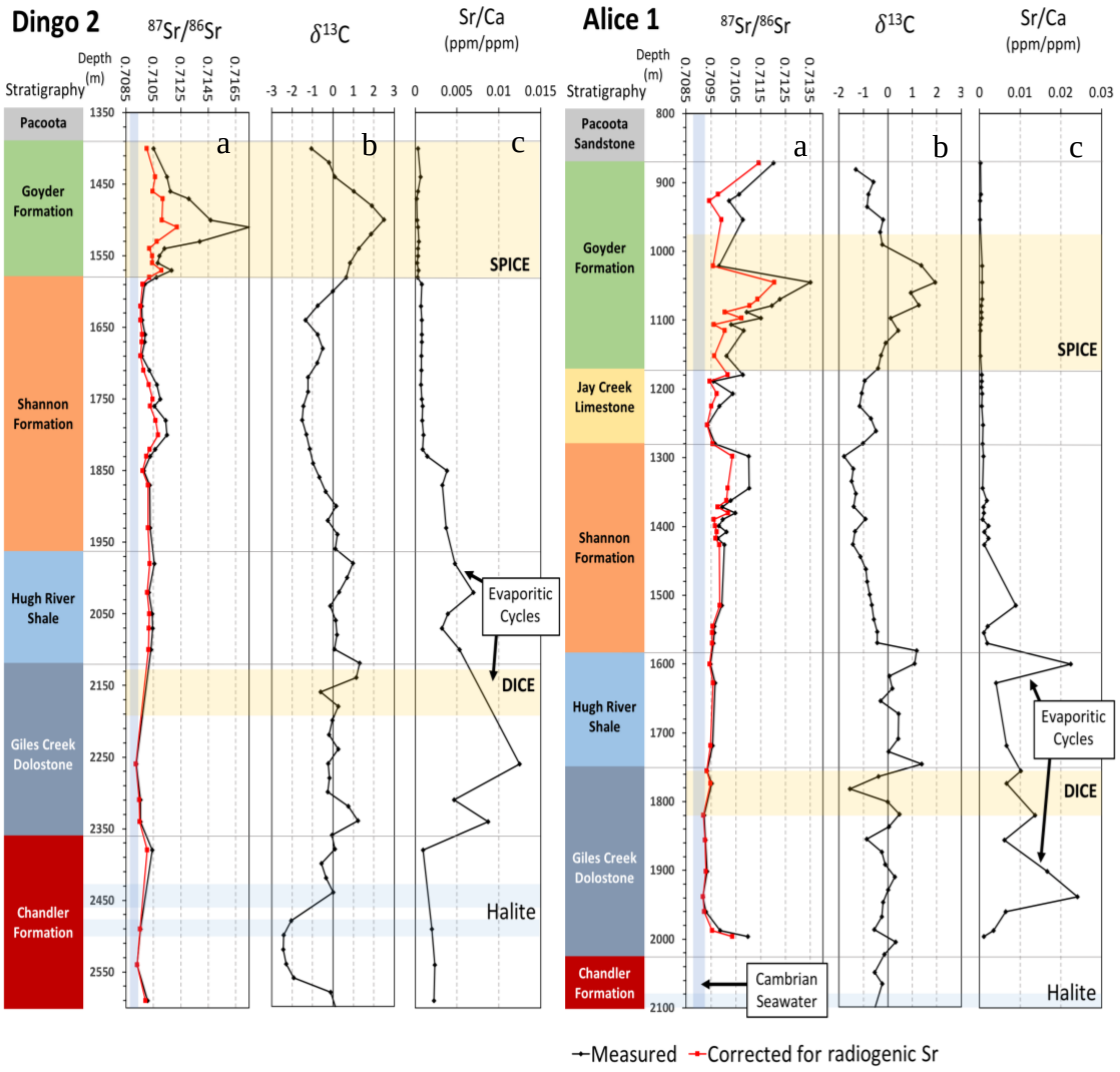

Figure 5. Sr and C isotopic trends and elemental Sr/Ca ratios of the Cambrian carbonate-rich sequences from the Amadeus Basin (from drill cores Dingo 2 and Alice 1. a) Strontium isotopic trend with expected Cambrian Seawater (0.7088-0.7093) indicated by the blue vertical rectangle (Black line indicates the measured $^{87}Sr/^{86}Sr$ values and the red line represents the measured data after applying the correction for in-situ Rb decay. b) Stable carbon $\delta^{13}C$ isotope data from Schmid (2017) and the yellow area show the SPICE and DICE C isotope anomalies. c) Sr/Ca ratio used as a proxy for evaporitic/gypsum cycles, which are also correlated with the abundance of celestine mineral ($SrSO_4$) in bulk carbonates, and thus with Sr/Ca ratios, as identified by Schmid (2017).

5. DISCUSSION

5.1 Evaluation of Diagenesis and Clay Contamination on the Primary Isotope Signals in Cambrian Marine Carbonates

The $^{87}Sr/^{86}Sr$ composition of marine carbonates can be used as (i) a tool for dating of sedimentary sequences based on the Sr isotope stratigraphy, and also (ii) as proxy for understanding of the tectonic evolution of our planet and the earth system over geological time (Elderfield, 1986; Shields, 2007; Veizer et al., 1999). However, the above applications could only be possible if the $^{87}Sr/^{86}Sr$ record of marine carbonates reflects the primary paleo-seawater composition, rather than some secondary processes such as clay contamination and/or meteoric diagenesis. The later can be assessed by plotting the Sr/Mn ratio against the $^{87}Sr/^{86}Sr$ ratio (shown in Figure 6), because primary and unaltered marine carbonates tend to have low Mn and high Sr concentrations while those affected by meteoric diagenesis and water/rock interactions tend to have low Sr and high Mn concentration (Banner and Hanson, 1990). Consequently, progressive diagenesis tends to lower Sr and increase Mn concentrations in altered carbonates until geochemical and isotope equilibrium with diagenetic/meteoric waters is reached (Edwards et al., 2015). On the other hand, clay contamination can be assessed by looking at the concentrations of Al and Rb in leached carbonate samples, as elevated concentrations of these elements are indicative of detrital phases and clay particles dissolution (Montañez et al., 1996).

Following these criteria, the best preserved carbonates should be those with hightest Sr/Mn (typically $\geq$ 0.5-2), low Rb/Sr (< 0.001) and low Al (< 10 ppm) concentrations, as these are most likely to record the primary marine $^{87}Sr/^{86}Sr$ signals (Edwards et al., 2015; Keller, Tennyson, Denison, Bohacs, & Survey, 1996; Montañez et al., 1996). Carbonate samples investigated in this study have generally elevated Al

concentrationa and Rb/Sr ratios (in excess of 0.001), which however might be also related to the fact that the studied depositional system is an intracratonic basin where one expects higher net inputs of continent-derived detrital material into the basin compared to more typical open ocean marine settings. However, samples from the stratigraphically lower successions (i.e., Giles Creek Dolostone and Chandler Formation) have the lowest Al concentrations and highest Sr/Mn ratios (Figure 3), and these are also carbonates that yield $^{87}Sr/^{86}Sr$ signatures that overlap with the expected Sr isotope composition of the coeval Cambrian oceans and paleo-seawater (Figure 5).

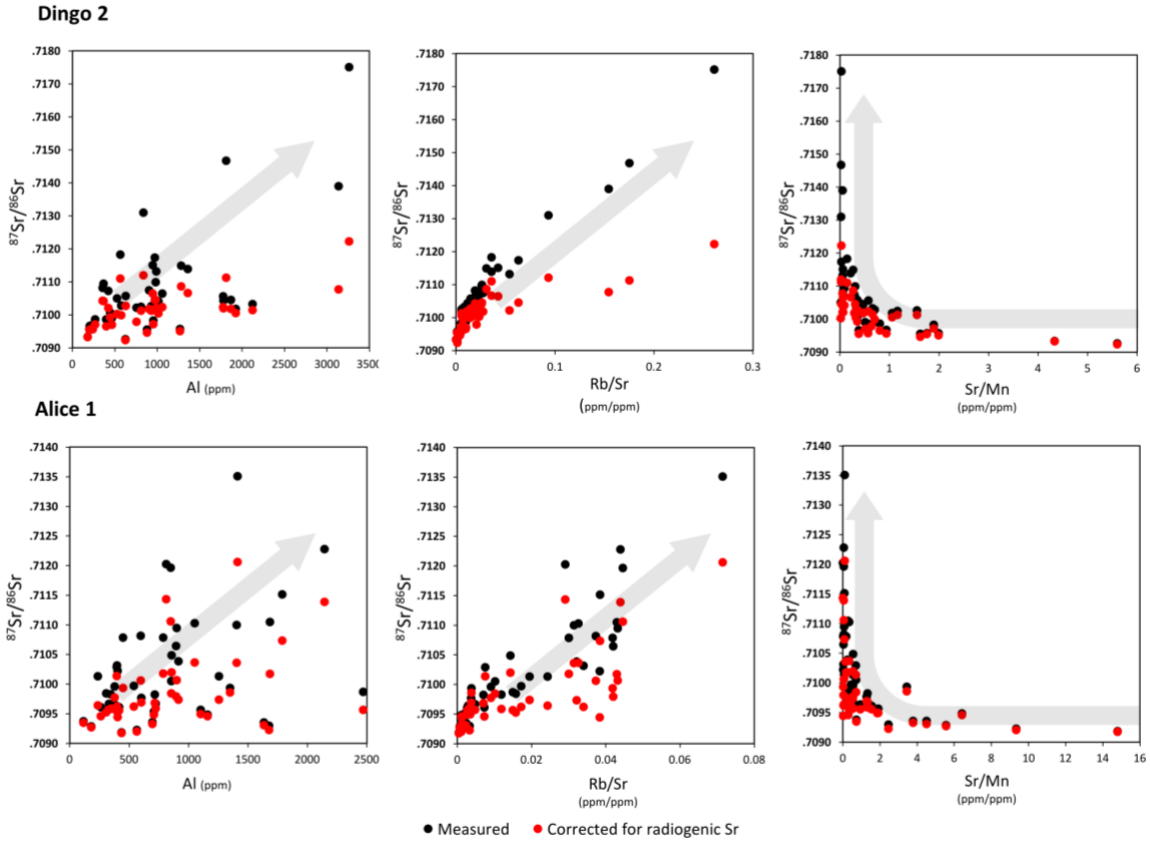

Figure 6. Cross plot of elemental concentrations and ratios versus Sr isotope signatures from carbonates collected from Dingo 2 and Alice 1. Left Diagrams) Al concentration vs. $^{87}Sr/^{86}Sr$ ratio, a grey arrow indicates increased clay contamination trend. Centre Diagrams) Rb/Sr vs. the $^{87}Sr/^{86}Sr$ ratios, a grey arrow indicates increased clay contamination . Right Diagrams) Sr/Mn ratio vs. $^{87}Sr/^{86}Sr$ data, a grey arrow indicates increased meteoric diagenesis.

5.2 Paleo-Redox Proxies in Marine Settings

Rare earth elements (REE) distribution in well-preserved marine carbonates can be used as tool to reconstruct paleo-redox conditions in marine environments during carbonate deposition (de Baar et al., 1988; Eltom, Abdullatif, & Babalola, 2017; Loope, Kump, & Arthur, 2013). Cerium in particular is important because it is redox sensitive REE, and when oxidized in a water column (from soluble Ce^{+3} to insoluble Ce^{+4}) it is then removed and absorbed from the water via precipitation on mineral surfaces and/or organic matter (Laenen, Hertogen, & Vandenberghe, 1997). Therefore, the Ce anomaly is defined by the extent Ce fractionates with respect to its neighbouring REE, such as La and Pr (see also Eq. 1). Hence, periods with elevated levels of oxygen in the ocean-atmosphere system will result in net depletion of Ce^{+3} in seawater, thus yielding a negative Ce anomaly in marine carbonates, as observed in the modern and oxygenated open ocean settings. On the other hand, under anoxic or oxygen-poor conditions Ce^{+4} is reduced to Ce^{+3}, resulting in a positive Ce anomaly in seawater (e.g., modern oxygen minimum zones) and precipitated carbonates. Note that La can behave anomalously and affect the calculated Ce anomaly (Ce/Ce*), thus the Pr anomaly (Pr/Pr*) should be also calculated and monitored to confirm that the observed Ce anomaly data are not analytical artifacts but rather true negative Ce/Ce* anomalies (Tostevin et al., 2016).

Schmid (2017) concluded that the Middle to Late Cambrian sedimentary record from the Amadeus Basin, represented by the stratigraphically younger Goyder and upper Shannon Formations, was deposited under anoxic conditions in a non-hypersaline marine settings, likely reflecting a progressive transgression and deepening of the local depositional environment. In contrast, the stratigraphically older successions, such as the Giles Creek Dolomite and Hugh River Formation, were deposited presumably under more oxygenated and shallow-marine to evaporitic settings associated with a regression

and sea-level lowstand (Schmid, 2017). An exception might be the Chandler Formation, which based on previous studies deposited under evaporitic and subaqueous anoxic conditions (Schmid, 2017, and references therein). This conclusion was based on the fact that the abundance of anhydrite (i.e. an evaporate with oxidised form of S) decreases and at the same time the abundance Fe mineral species change from hematite (oxidised form of Fe) to pyrite (reduce Fe) throughout the studied section.

To further test such proposed marine redox changes in the Amadeus Basin during the studied Cambrian interval, we present in Figure 7 a cross-plot of Ce/Ce* versus Pr/Pr* anomaly data that were compiled from carbonates/formations collected and analysed in both cores (Alice 1 and Dingo 2). Interestingly, all samples from the stratigraphically younger Goyder Formation appear to display positive Ce/Ce* anomaly, which are thus in agreement with the proposed reducing conditions during the deposition (see above and Schmid, 2017). The Shannon Formation samples also suggest relatively reducing environments but the calculated Ce/Ce* anomaly data are not as positive (i.e., anoxic) as those found in the Goyder Formation samples (see Figure 7). The Giles Creek Dolostone samples appear to be scattered around the PAAS values, some exhibiting true negative Ce/Ce* anomaly and some positive La anomaly, two samples lie within the boundary of positive Ce/Ce* anomaly. Finally, two samples from the Chandler Formation exhibit a true negative Ce/Ce* anomaly, thus suggesting more oxic conditions during these times, which also agrees with the proposition of Schmid (2017). Overall, data in Figure 7 show evidence for a progressive changes in marine redox from relatively reducing/anoxic conditions to more oxic settings moving down the stratigraphy. This trend is in a general agreement with a hypothesised paleo-redox scenario for this time interval as proposed by Schmid (2017) and others.

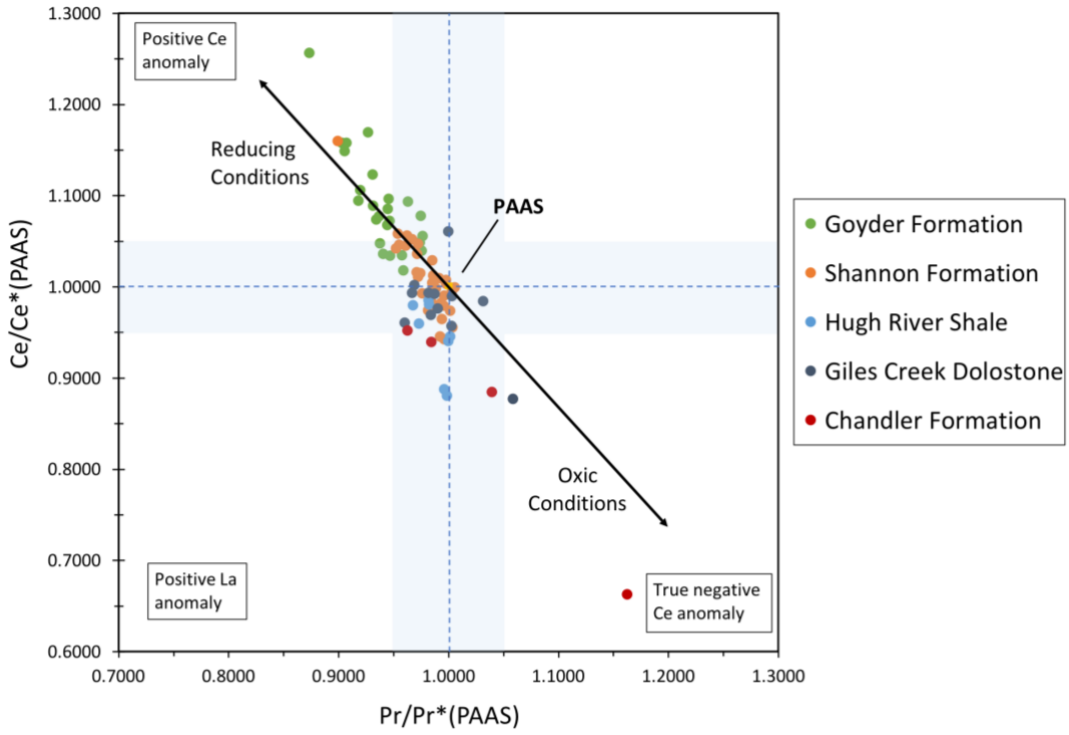

Figure 7. A cross-plot of shale-normalized (PAAS) Ce/Ce* and Pr/Pr* anomalies of the studied middle Cambrian carbonates from the NE parts of the Amadeus Basin.

5.3 Sr Isotope Constraints on Paleo-Depositional Environment

Apart from the application of $^{87}Sr/^{86}Sr$ for the Strontium isotopes stratigraphy (SIS) of marine carbonates (McArthur et al., 2012), this isotope tracer can be also used to infer changes in the paleo-depositional environment of carbonate deposits, assuming that the approximate age of these samples is known or can be constrained by other means (e.g. biostratigraphy, UPb dating, etc). Specifically, the $^{87}Sr/^{86}Sr$ proxy can be used to distinguish between normal marine settings from the restricted (evaportic, brackish) coastal environments, thus providing information about the relative connectivity of the basin with respect to the open ocean (Zhao et al., 2009). This is based on the fact that the $^{87}Sr/^{86}Sr$ ratio in the ocean is homogeneous at any given time due to its long residence time (>1 Ma) relative to the typical mixing time of the global ocean (~1500 a). The $^{87}Sr/^{86}Sr$ ratio of the Cambrian ocean was highly affected by the Pan-African orogeny and ranged from 0.7088 to 0.7093 (McArthur et al., 2012;

Montañez et al., 1996; Peng et al., 2012). Thus, any variations from the expected $^{87}Sr/^{86}Sr$ composition of the global Cambrian ocean might indicate local effects related to a possible restriction of a depositional system (e.g., intracratonic basin, lagoon, etc) from the open ocean, where the basin becomes impacted by inputs of more radiogenic Sr from the continents. For example, Sr supplied from continental weathering by rivers has a high $^{87}Sr/^{86}Sr$ ratio of ~0.711, while Sr originating from the submarine dissolution and recrystallization of carbonate has intermediate $^{87}Sr/^{86}Sr$ ratio of ~0.708 (Wierzbowski, 2013).

EVAPORITIC CYCLES AND CONSTRAINTS ON THE RESTRICTION OF THE BASIN

The advancement in chronostratigraphy and biostratigraphy provides time-specific patterns of biofacies and lithofacies throughout the Cambrian (Babcock et al., 2015). Schmid (2017) identified a transgressive 2nd order cyclicity, with multiple 3rd order cycles, in the Cambrian sedimentary record of the Amadeus Basin (between 511 to 490 Ma). The above 3rd order cycles were defined mainly based on the cyclic deposition of HST (highstand systems tract) carbonate rocks and LST (lowstand systems tract) fine grained siltstones across all the studied successions. The abundance of calcite and dolomite versus phyllosilicates, feldspar and quartz was also used to determine the cyclicity with the use of CaO/SiO_2 ratio as an additional tool. Schmid (2017) interpreted the cyclicity to be related to evaporite cycles similar to the evaporitic cycles during the Permian in the Zechstein basin and proposed deposition as salina or evaporitic seaway based on several geochemical and biological indicators. Moreover, Schmid (2017) was able to successfully correlate the above cyclicity pattern not only across the Cambrian sequences from the Amadeus Basin, but also with the global Cambrian cyclicity record compiled by (Babcock et al., 2015).

Importantly, the acquired $^{87}Sr/^{86}Sr$ data from this study show consistent Sr isotope trends in both investigated cores (Alice 1 and Dingo 2), suggesting basin wide signals, as shown in Figure 5. In addition, two of the evaporitic cycles put forward by Schmid (2017) can be also observed in our Sr/Ca data (as a proxy for celestine: $SrSO_4$ mineral, see Figure 5), which is a mineral that is associated with evaporitic sequences (Schmid, 2017). Interestingly, the corresponding $^{87}Sr/^{86}Sr$ ratios of carbonates from these evaporitic cycles (lower Shannon to Chandler Formations) are identical or close to the expected Sr isotope composition of Cambrian seawater (Figure 5). Similarly, $^{87}Sr/^{86}Sr$ data from the Giles Creek Dolostone lie within the expected Cambrian seawater values, suggesting limited restriction of the basin during the deposition of these evaporitic cycles proposed by Schmid (2017). This in turn requires depositional environment with some level of connectivity to the Cambrian open ocean, supporting an "evaporitic seaway" model rather than "salina" model for the formation of these evaporitic/shallow water carbonates in the Amadeus Basin. In addition, a recent study by (Hearing et al., 2018) proposed an average Earth's surface temperatures of 30-45°C at low latitudes during the early Cambrian (~514 to 509 Ma), and during this time Australia was presumably located near the equator (Hearing et al., 2018; Torsvik 2016). Thus, the equatorial position of the Australia (and by inference the Amadeus Basin, Figure 8), coupled with the Cambrian greenhouse/hothouse climate (Hearing et al. 2018), can explain the formation of larger scale low-latitude evaporitic seaways systems, which are supported by Sr isotope data presented in this study.

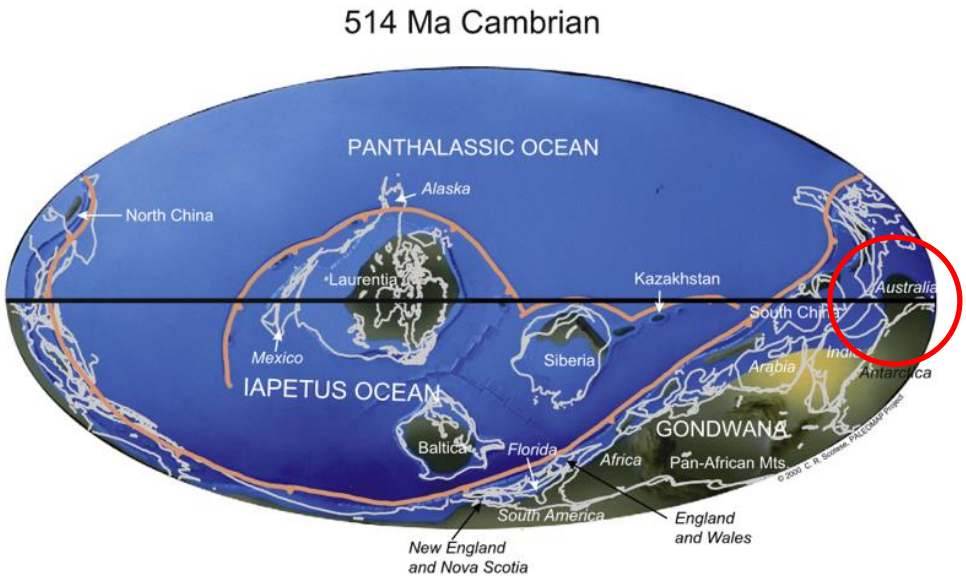

Figure 8. Global paleo-geography map of the Cambrian period (514 Ma) showing the location of Australia (and thus the Amadeus Basin) near the equator (Peng et al., 2012).

THE STEPTOEAN POSITIVE CARBON ISOTOPE EXCURSION (SPICE)

Major bioevents during the Cambrian period coincide with several positive and negative excursions in the marine carbonate $\delta^{13}C$ record, and there are in total 4 major carbon isotope excursions recorded globally during the Cambrian (Fan, Deng, & Zhang, 2011). Specifically, these are listed below from stratigraphically oldest (negative excursion) to youngest (positive excursions): BACE (BAsal Cambrian Carbon Isotope Excursion), ZHUCE (ZHUjiaqing Carbon Isotope Excursion), MICE (MIngxinsi Carbon Isotope Excursion), and SPICE (Steptoean Positive Carbon Isotope Excursion). The SPICE is the main focus in this study, and this major positive C isotope excursion occurs in the Paibian Stage at the base of the Furongian Series spanning 3.5 Ma (499-495.5 Ma). The SPICE was documented globally from different paleocontinents and locations, including Kazakhstan, Siberia, China, Australia and North America, with typical average $\delta^{13}C$ amplitude of 4‰, rising from $\pm$1‰ to reach 3-5‰ (Fan et al., 2011).

The origin of the SPICE and its links to Cambrian biological evolution are highly controversial and discussed matters, and generally two main mechanisms or processes have been proposed to explain this globally recognised C isotope positive excursion (see Schmid, 2017, and references therein). First hypothesis suggests an increase in the burial of organic carbon in the oceans due to fall of sea level which would increase weathering and erosion and thus providing an increasing input of nutrients the ocean, thus increasing its fertility and as consequence also the primary productivity. This in turn will result in an increase in the organic carbon burial and thus removal of ^{12}C from seawater, leading to a formation of positive marine $\delta^{13}C$ excursion. However, there is no convincing evidence for enhanced deposition of black shales (organic matter) in geological record during this time period that would to support such scenario (Schmid, 2017, Fan, Deng, & Zhang, 2011). Alternative hypothesis suggests that the formation of methane hydrates due to a global cooling could have removed efficiently ^{12}C from the oceans leading to the formation of positive excursion (SPICE). Recent oxygen isotope constraints on Cambrian climate are however at odds with such alternative scenario, as new $\delta^{18}O$ data from well-preserved fossils suggest a greenhouse climate rather than cooling (Hearing et al., 2018).

A basin-wide record of the SPICE event across the Amadeus Basin was documented recently by (Schmid et al., 2018), and the latter study also observed an increased ratio of siliciclastic to carbonate rocks in some of the studied sections across the SPICE peak. (Schmid et al., 2018) stated two opposing models to explain this increase. The first model by (Osleger & Read, 1993) suggests a transgression during the SPICE resulting in drowning of the carbonate platform and deposition of siliciclastic rocks thus increasing the siliciclastic to carbonate rocks ratio. The second model suggested an increased weathering rate during a regression causing an increase in the

burial of organic carbon in siliciclastic rocks due to the increase in continental input of nutrients (Schmid et al., 2018). Based on litholological and mineralogical evidence, Schmid et al. (2018) concluded that the increase in siliciclastics to carbonate phases during the SPICE peak in the Amadeus Basin is due to change in climate from arid to humid. The latter would cause a change and increase in continental weathering flux into the ocean during transgression. Importantly, Figure 9a shows positive correlation between the $^{87}Sr/^{86}Sr$ and $\delta^{13}C$ data during the SPICE, which supports a scenario of increased continental inputs and weathering fluxes into the basin during this positive C isotope excursion, which might imply a regression during the SPICE event. On the other hand, Figure 9b shows a negative correlation between the Ce/Ce* and $\delta^{13}C$ data from studied samples during the SPICE, suggesting associated redox changes. However, the Ce/Ce* anomaly remains positive throughout the SPICE event suggesting generally anoxic conditions, which in turn might indicate deepening of the depositional environment possibly linked to a transgression rather than the before mentioned regression. Interestingly, the onset of the SPICE coincides with the most positive Ce/Ce* anomaly (~1.3), followed by a systematic decrease in the Ce/Ce* with increasing $\delta^{13}C$ values (Figure 9). This might suggest progressively less reducing (or more oxic) conditions during the peak of SPICE event, possibly due to enhanced O_2 production in the basin as a consequence of increased organic carbon burial. Overall, combining the Ce/Ce* anomaly and $^{87}Sr/^{86}Sr$ data from studied carbonates, the SPICE event in the Amadeus Basin most likely occurred during a period of marine transgression (or deepening of the basin) that was accompanied by increased continental weathering fluxes, possibly linked to climate changes (from arid to more humid) as suggested by Schmid (2017).

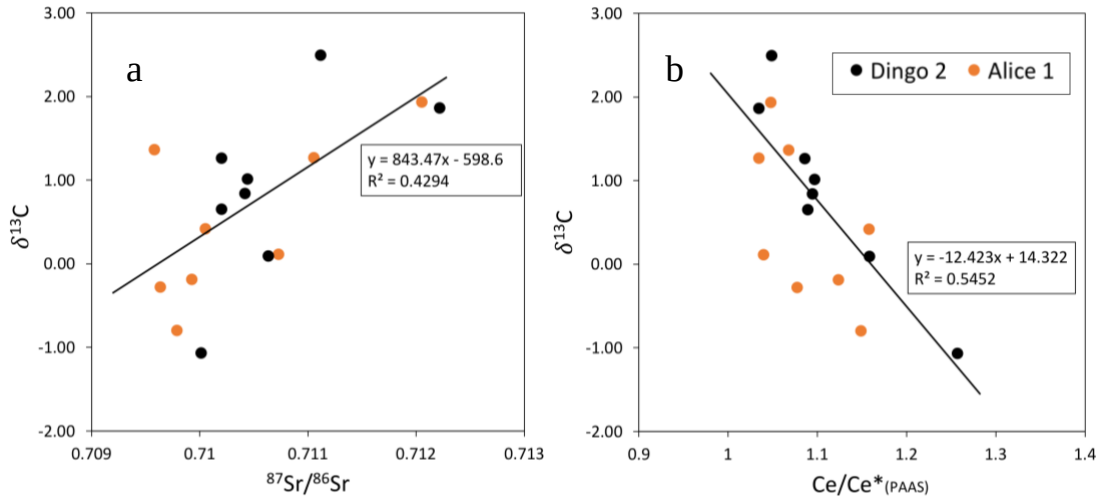

Figure 9. a) The $^{87}Sr/^{86}Sr$ ratio plotted against the $\delta^{13}C$ during the SPICE anomaly (Paibian stage) showing a positive correlation. b) The shale-normalized (PAAS) Ce anomaly plotted against the $\delta^{13}C$ during the SPICE anomaly showing negative correlation.

5.4 CORRELATION WITH $^{87}SR/^{86}SR$ GLOBAL CURVE

The $^{87}Sr/^{86}Sr$ values of the Cambrian carbonates from the Amadeus Basin were compared with the published middle Cambrian paleo-seawater Sr isotope record (Figure 10), the latter based on the compilation of 166 published data points collected from different studies and representing globally distributed paleo-locations and sampling sites (Denison, Koepnick, Burke, & Hetherington, 1998; Ebneth, Shields, Veizer, Miller, & Shergold, 2001; Qing, Barnes, Buhl, & Veizer, 1998). Samples from this study were given an approximate age based on their depth and stratigraphy, following also the Cambrian chronostratigraphy of the Amadeus Basin from Schmid (2017). Generally, the Sr isotope record produced by this study is systematically more radiogenic compared to the expected middle Cambrian seawater $^{87}Sr/^{86}Sr$ trend (data in blue rectangle in Figure 10), except the lower successions of the middle Cambrian record (Giles Creek Dolostone and the Chandler Formation) which both show some data that are very close or even overlap to the coeval Cambrian paleo-seawater record ($^{87}Sr/^{86}Sr$ of ~0.7088 to ~0.7093). Importantly, Figure 10 also illustrates progressive restriction of

the Amadeus Basin from the global ocean moving up the middle Cambrian stratigraphy, accompanied also by enhanced inputs of continent-derived Sr weathering fluxes into the basin.

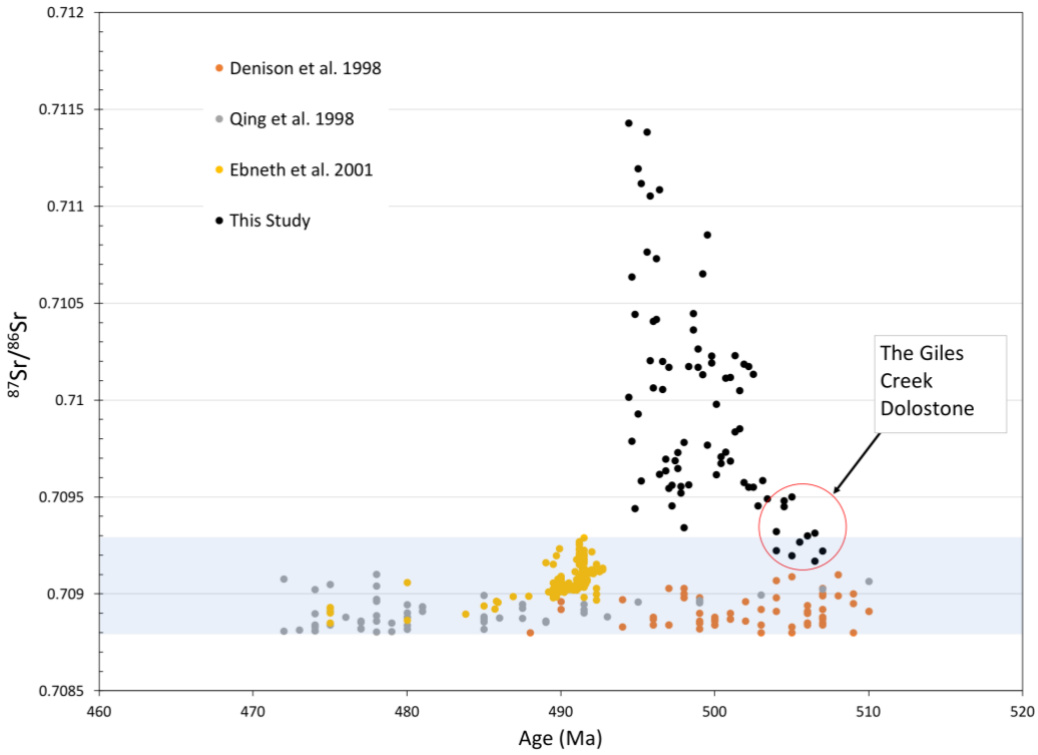

Figure 10. Compilation of published $^{87}Sr/^{86}Sr$ record of paleo-seawater or global ocean during middle to upper Cambrian (~510 to ~485 Ma), which is compared to coeval Sr isotope record from the Amadeus Basin (black circles = this study). Note that The Giles Creek Dolostone samples shown by the red circle lie within or very close to the expected $^{87}Sr/^{86}Sr$ range of middle Cambrian seawater, the latter indicated by the blue rectangle.

6. CONCLUSIONS

The paleo-depositional environment and past marine redox conditions in the NE parts of the Amadeus Basin during the middle Cambrian (~515 to ~495 Ma) were constrained based on the Sr isotope and REE analysis of carbonates from two remote drill cores: Dingo 2 and Alice 1. The REE data, particularly Ce/Ce* anomaly, show an evidence of relatively reducing and O_2-poor marine conditions in the basin that progressively change to more oxic redox conditions moving down the stratigraphy. As to Sr isotopes, the acquired $^{87}Sr/^{86}Sr$ record of the lower successions (Giles Creek

Dolostone and the Chandler Formation) is consistent or very close to the middle Cambrian global paleo-seawater $^{87}Sr/^{86}Sr$ trend, suggesting that the Amadeus Basin was at some level connected to the open ocean during this time. However, evidence of several evaporitic cycles in this record, suggest that such connectivity had to be likely facilitated via "evaporitic seaway" settings rather than reflecting true and barrier free connection between the Amadeus Basin and coeval open ocean. The presence of evaporitic cycles with normal marine Sr isotope signatures also further supports the existence of middle Cambrian greenhouse climate conditions, and the equatorial position of Australia (and thus the Amadeus Basin) during this time also suggests an intense evaporation of the equatorial and low-latitude ocean water masses. However, the $^{87}Sr/^{86}Sr$ record of the Amadeus Basin becomes increasingly more radiogenic in the younger and/or upper carbonate successions (i.e., the Shannon and Goyder Formations), where the data indicate a massive increase in continental-weathering fluxes into the basin and its more significant restriction from the Cambrian oceans. In addition, REE data (Ce/Ce* anomaly) from these younger successions also imply that the coeval positive C isotope excursion (SPICE anomaly) occurred during more reducing paleo-redox marine conditions, likely pointing to a progressive transgression or deepening of the depositional environment during SPICE. Combining the findings from this study, the SPICE anomaly most likely occurred during a marine transgression with increasing continental weathering fluxes due to ongoing change in climate from arid to more humid conditions.

ACKNOWLEDGMENTS

First and foremost, a big thank you to my supervisor Dr. Juraj Farkas for his patience, efforts and guidance over this year. Special thanks to David Bruce, Tony Hall and Sarah Gilbert for their constant help and the time they gave. Lastly, a big thank you to

Susanne Schmid at CSIRO Mineral Resources for providing the samples. This work has been funded and supported by NTGS and could not have occurred without their most generous contribution. Lastly, thanks to all my fellow honour students for their help through this year.

REFERENCES

Ahmad , M., & Munson , T. (2013). Geology and mineral resources of the Northern Territory. *Geology and mineral resources of the Northern Territory*(Special publication 5).

ASUD. (2018). *Australian Stratigraphic Units Database*.

Babcock, L., Peng, S., Brett, C., Zhu, M., Ahlberg, P., Bevis, M., & Robison, R. (2015). Global climate, sea level cycles, and biotic events in the Cambrian Period. *ScienceDirect*.

Bau, M., & Dulski, P. (1996). Distribution of yttrium and rare-earth elements in the Penge and Kuruman iron-formations, Transvaal Supergroup, South Africa. *Precambrian Research, 79*(1), 37-55. doi:https://doi.org/10.1016/0301-9268(95)00087-9

de Baar, H. J. W., German, C. R., Elderfield, H., & van Gaans, P. (1988). Rare earth element distributions in anoxic waters of the Cariaco Trench. *Geochimica et Cosmochimica Acta, 52*(5), 1203-1219. doi:https://doi.org/10.1016/0016-7037(88)90275-X

Denison, R., Koepnick, R., Burke, W., & Hetherington, E. (1998). Construction of the Cambrian and Ordovician seawater 87Sr/86Sr curve. *Chemical Geology, 152*(3-4), 325-340.

Ebneth, S., Shields, G. A., Veizer, J., Miller, J. F., & Shergold, J. H. (2001). High-resolution strontium isotope stratigraphy across the Cambrian-Ordovician transition. *Geochimica et Cosmochimica Acta, 65*(14), 2273-2292. doi:https://doi.org/10.1016/S0016-7037(01)00580-4

Edwards, C. T., Saltzman, M. R., Leslie, S. A., Bergström, S. M., Sedlacek, A. R. C., Howard, A., . . . Young, S. A. (2015). Strontium isotope (87 Sr/ 86 Sr) stratigraphy of Ordovician bulk carbonate: Implications for preservation of primary seawater values. *Geological Society of America Bulletin, 127(9-10)*, pp. 1275-1289.

Elderfield, H. (1986). Strontium isotope stratigraphy. *Palaeogeography, Palaeoclimatology, Palaeoecology, 57*(1), 71-90. doi:https://doi.org/10.1016/0031-0182(86)90007-6

Eltom, H. A., Abdullatif, O. M., & Babalola, L. O. (2017). Redox conditions through the Permian-Triassic transition in the upper Khuff formation, Saudi Arabia. *Palaeogeography, Palaeoclimatology, Palaeoecology, 472*, 203-215. doi:https://doi.org/10.1016/j.palaeo.2017.01.046

Fan, R., Deng, S., & Zhang, X. (2011). Significant carbon isotope excursions in the Cambrian and their implications for global correlations. *Science China Earth Sciences, 54*(11), 1686. doi:10.1007/s11430-011-4313-z

Hearing, T. W., Harvey, T. H. P., Williams, M., Leng, M. J., Lamb, A. L., Wilby, P. R., . . . Donnadieu, Y. (2018). An early Cambrian greenhouse climate. *Science Advances, 4*(5).

Jarrett, A., Edwards, D., Boreham, C., & McKirdy, D. (2016). *Petroleum geochemistry of the Amadeus Basin*. Paper presented at the AGES 2016, Alice Springs, Northern Territory

Keller, M. A., Tennyson, M. E., Denison, R. E., Bohacs, K. M., & Survey, G. (1996). *Strontium Isotope Evidence for the Age of the Vaqueros Formation and Latest Oligocene Marine Transgression in the Northern Santa Maria Province, Central California*: U.S. Government Printing Office.

Kennard, J. M., & Korsch, R. J. (2017). *Geological and geophysical studies in the Amadeus Basin, central Australia*. Canberra: Australian Government Publishing Service.

Krabbenhöft, A., Fietzke, J., Eisenhauer, A., Liebetrau, V., Böhm, F., & Vollstaedt, H. (2009). Determination of radiogenic and stable strontium isotope ratios (87Sr/86Sr; δ88/86Sr) by thermal ionization mass spectrometry applying an 87Sr/84Sr double spike. *Journal of Analytical Atomic Spectrometry, 24*(9), 1267-1271. doi:10.1039/B906292K

Laenen, B., Hertogen, J., & Vandenberghe, N. (1997). The variation of the trace-element content of fossil biogenic apatite through eustatic sea-level cycles. *Palaeogeography, Palaeoclimatology, Palaeoecology, 132*(1), 325-342. doi:https://doi.org/10.1016/S0031-0182(97)00068-0

Liu, C., Wang, Z., & Raub, T. D. (2013). Geochemical constraints on the origin of Marinoan cap dolostones from Nuccaleena Formation, South Australia. *Chemical Geology, 351*, 95-104. doi:https://doi.org/10.1016/j.chemgeo.2013.05.012

Loope, G. R., Kump, L. R., & Arthur, M. A. (2013). Shallow water redox conditions from the Permian–Triassic boundary microbialite: The rare earth element and iodine geochemistry of carbonates from Turkey and South China. *Chemical Geology, 351*, 195-208. doi:https://doi.org/10.1016/j.chemgeo.2013.05.014

Marshall, T. (2005). *Review of source rocks in the Amadeus Basin* (NTGS Record 2004-008). Retrieved from

McArthur, J., Howarth, R., & Shields, G. (2012). Strontium isotope stratigraphy. In *The geologic time scale* (pp. 127-144): Elsevier.

Montañez, I. P., Banner, J. L., Osleger, D. A., Borg, L. E., & Bosserman, P. J. (1996). Integrated Sr isotope variations and sea-level history of Middle to Upper Cambrian platform carbonates: Implications for the evolution of Cambrian seawater 87Sr/86Sr. *Geology, 24*(10), 917-920.

Munson, T. (2014). *Petroleum geology and potential of the onshore Northern Territory 2014*. Retrieved from

Nance, W. B., & Taylor, S. R. (1976). Rare earth element patterns and crustal evolution—I. Australian post-Archean sedimentary rocks. *Geochimica et Cosmochimica Acta, 40*(12), 1539-1551. doi:https://doi.org/10.1016/0016-7037(76)90093-4

Nurgalieva, N. G., Ponomarchuk, V. A., & Nurgaliev, D. K. (2007). Strontium isotope stratigraphy: Possible applications for age estimation and global correlation of Late Permian carbonates of the Pechishchi type section, Volga River. *Russian Journal of Earth Sciences., 9*(Russian Journal of Earth Sciences.). doi:10.2205/2007ES000221

Osleger, D., & Read, J. F. (1993). Comparative analysis of methods used to define eustatic variations in outcrop: Late Cambrian interbasinal sequence development. *American Journal of Science, 293*(3), 157-216.

Paces, J. B., Peterman, Z. E., Futa, K., Oliver, T. A., & Marshall, B. D. (2007). Strontium isotopic composition of paleozoic carbonate rocks in the Nevada Test Site vicinity, Clark, Lincoln, and Nye Counties, Nevada, and Inyo County, California. *U.S. Geological Survey Data Series 280*.

Peng, S., Babcock, L. E., & Cooper, R. A. (2012). Chapter 19 - The Cambrian Period. In F. M. Gradstein, J. G. Ogg, M. D. Schmitz, & G. M. Ogg (Eds.), *The Geologic Time Scale* (pp. 437-488). Boston: Elsevier.

Purdy, D. J., Cross, A. J., Brown, D. D., Carr, P. A., & Armstrong, R. A. (2016). New constraints on the origin and evolution of the Thomson Orogen and links with central Australia from isotopic studies of detrital zircons. *Gondwana Research, 39*, 41-56. doi:https://doi.org/10.1016/j.gr.2016.06.010

Qing, H., Barnes, C., Buhl, D., & Veizer, J. (1998). *The strontium isotopic composition of Ordovician and Silurian brachiopods and conodonts: Relationships to geological events and implications for coeval seawater* (Vol. 62).

Schmid, S. (2017). Chemostratigraphy and palaeo-environmental characterisation of the Cambrian stratigraphy in the Amadeus Basin, Australia. *Chemical Geology, 451*, 169-182.

Schmid, S., Smith, P. M., & Woltering, M. (2018). A basin-wide record of the Late Cambrian Steptoean positive carbon isotope excursion (SPICE) in the Amadeus Basin, Australia.

Palaeogeography, Palaeoclimatology, Palaeoecology, 508, 116-128. doi:https://doi.org/10.1016/j.palaeo.2018.07.027

Shields, G. A. (2007). A normalised seawater strontium isotope curve: possible implications for Neoproterozoic-Cambrian weathering rates and the further oxygenation of the Earth. *eEarth, 2(2)*, 35-42. doi:10.5194/ee-2-35-2007

Taylor, S. R., & McClennan, S. M. (1985). The Continental Crust: Its Composition and Evoution. 312.

Tostevin, R., Shields, G. A., Tarbuck, G. M., He, T., Clarkson, M. O., & Wood, R. A. (2016). Effective use of cerium anomalies as a redox proxy in carbonate-dominated marine settings. *Chemical Geology, 438*, 146-162. doi:https://doi.org/10.1016/j.chemgeo.2016.06.027

Veizer, J., Ala, D., Azmy, K., Bruckschen, P., Buhl, D., Bruhn, F., . . . Strauss, H. (1999). 87Sr/86Sr, δ13C and δ18O evolution of Phanerozoic seawater. *Chemical Geology, 161*(1), 59-88. doi:https://doi.org/10.1016/S0009-2541(99)00081-9

Webb, G., Nothdurft, L., Kamber, B., Kloprogge, T., & Zhao, J.-x. (2009). Rare earth element geochemistry of scleractinian coral skeleton during meteoric diagenesis: A sequence through neomorphism of aragonite to calcite. *Sedimentology, 56*(5), pp. 1433-1463.

Webb, G. E., & Kamber, B. S. (2000). Rare earth elements in Holocene reefal microbialites: a new shallow seawater proxy. *Geochimica et Cosmochimica Acta, 64*(9), 1557-1565. doi:https://doi.org/10.1016/S0016-7037(99)00400-7

Wierzbowski, H. (2013). Strontium isotope composition of sedimentary rocks and its application to chemostratigraphy and palaeoenvironmental reconstructions. *ANNALES UMCE, 68(1)*. doi:http://dx.doi.org/10.2478/v10246-012-0017-2

Zhao, Y.-Y., Zheng, Y.-F., & Chen, F. (2009). Trace element and strontium isotope constraints on sedimentary environment of Ediacaran carbonates in southern Anhui, South China. *Chemical Geology, 265*(3), 345-362. doi:https://doi.org/10.1016/j.chemgeo.2009.04.015

APPENDIX A: EXTENDED METHODS

Solution QQQ

Sample solutions were analysed at Adelaide Microscopy, Adelaide University, with an Agilent 8900x QQQ-ICP-MS. The plasma conditions were: RF power 1550W, sample depth 8mm and Ar carrier gas flow rate 1.09 L/min, with a Micro Mist nebuliser and Scott Type spray chamber. The collision cell was run in He mode (4 mL/min He gas flow) for the majority of elements [K, Rb, Sr, Al, Ti, Cr, Mn, Fe, Cu, S, P, Mg, Ca and all REE]. Li was analysed in No-Gas mode for improved detection limits. Si, P, Ca and Fe were analysed with Oxygen (30% flow rate) in the collision cell and the MO+ reaction products measured for each element: 28Si → 28Si16O measured at mass 44; 31P → 31P16O at mass 47; 44Ca → 44Ca16O at mass 60; and 56Fe → 56Fe16O at mass 72). On-line addition of In was used as the internal standard element. A series of mixed element calibration solutions [0, 10, 20, 50, 100, 200 and 500 ppb] were used for quantification. The JDo-1 was used as a quality control standard.

$^{87}Sr/^{86}Sr$ isotope analysis extended methods

The strontium was separated using ion chromatography in polyprep columns containing

Eichrom Sr resin SPS, using the following method:

1) Wash resin and column with 3 ml of 8M HNO_3 sd
2) Wash resin and column with 3 ml of DI H_2O
3) Wash resin and column with 3 ml of 8M HNO_3 sd
4) Wash resin and column with 3 ml of DI H_2O
5) Wash resin and column with 3 ml of 8M HNO_3 sd
6) Load Samples in 1 ml 8M HNO_3 sd
7) 5 x wash with 1 ml of 8M HNO_3 sd
8) Collect SR with 6 x 0.05M HNO_3 sd
9) Add 1 drop of H_3PO_4 to Sr vial and spike any blanks
10) Dry on hot plate at 140°C
11) Add squirt of 15M HNO_3 sd to oxidise any organics
12) Cap vials and heat at 110°C for at least 5 hours
13) Dry on hotplate at 140°C.

APPENDIX B: CALCULATIONS

Cerium Anomaly Calculation

The shale-normalized cerium anomaly (Ce/Ce*) was calculated based on the equation from (G. E. Webb & Kamber, 2000), (modified after (Bau & Dulski, 1996)

$$Ce/Ce^* = [Ce/Ce_{(PAAS)}] / [0.5 \times (La/La_{(PAAS)}) + 0.5 \times (Pr/Pr_{(PAAS)})]$$

where PAAS is the "Post-Archean Average Australian Shale" and its REE composition is shown in table below:

Sample ID	La	Ce	Pr	Nd	Sm	Eu	Gd	Tb	Dy	Ho	Er	Tm	Yb	Lu
PAAS (ppm)	38	80	8.9	32	5.6	1.1	4.7	0.8	4.4	1.0	2.9	0.4	2.8	0.4

(Nance & Taylor, 1976)

Praseodymium Anomaly Calculation

The shale-normalized Praseodymium anomaly (Pr/Pr*) was calculated in similar way based on the equation below :

$$Pr/Pr^* = [Pr/Pr_{(PAAS)}] / [0.5 \times (Ce/Ce_{(PAAS)}) + 0.5 \times (Nd/Nd_{(PAAS)})]$$

APPENDIX C: FULL DATA SET

Table 1: Colours representing the different lithologies to be used for referencing all future tables.

	Goyder formation
	Shannon formation
	Hugh River Shale
	Giles Creek Dolostones
	Chandler formation

Table 2: Dingo 2 data set of major and trace elements.

Depth (m)	Mg_ppm	Ca_ppm	Li_ppm	Al_ppm	Si_ppm	P_ppm	K_ppm	Ca_ppm	Sc_ppm	Ti_ppm	V_ppm	Cr_ppm	Mn_ppm	Fe_ppm
1400	113662.541	195570.787	0.561	529.071	1632.187	389.437	228.219	163958.652	1.290	5.151	8.260	37.127	2368.084	29808.687
1440	100693.540	179843.823	1.367	949.382	1582.485	504.955	682.928	154191.773	3.880	9.535	9.211	25.344	1634.822	26732.804
1460	106667.701	189972.414	1.021	974.709	1242.220	121.554	454.979	159707.703	2.654	10.951	5.262	11.603	1638.632	22452.059
1470	105900.893	186074.609	1.496	840.521	1718.967	168.549	634.988	156653.040	1.787	24.936	6.004	3.629	1060.030	8654.384
1500	94321.906	162484.480	1.988	1816.537	2838.253	86.299	1182.964	140809.429	4.898	27.501	7.776	15.569	1391.780	23994.611
1510	73540.928	132898.988	3.072	3263.710	4363.514	875.712	1898.752	112924.757	4.536	60.186	12.363	5.725	1080.413	8718.334
1530	92029.329	165699.801	4.360	3139.501	4894.701	400.147	1817.058	143637.124	6.698	76.305	15.212	5.665	1108.688	12382.391
1540	111922.155	210046.040	1.396	992.023	1804.923	34.371	580.982	165721.558	3.458	12.092	5.223	14.982	995.724	22420.103
1550	90778.466	179307.410	0.651	369.301	670.335	86.322	262.021	134880.293	1.631	12.632	5.512	3.441	594.035	7858.105
1560	135983.856	233562.363	0.672	360.558	546.096	56.239	162.908	197375.127	2.118	2.476	7.742	11.495	807.487	12568.058
1570	94992.455	220143.200	1.432	569.769	1067.491	149.801	462.755	183485.788	2.364	19.237	7.351	2.880	521.656	5659.880
1580	103500.261	193197.558	0.560	426.146	519.193	57.687	181.217	162098.472	2.148	3.889	5.232	7.431	629.921	10811.262
1590	39894.109	189431.236	0.632	271.695	498.807	81.154	175.202	155310.496	1.618	8.299	4.393	1.939	266.826	3589.334
1620	53583.127	192372.473	0.399	208.945	369.115	18.259	95.706	158274.076	1.691	1.351	3.923	3.771	294.054	5503.210
1640	33324.733	249472.285	0.580	231.083	335.471	15.199	122.323	212254.081	2.468	3.059	3.082	3.966	299.171	4338.192
1660	49689.546	188042.038	0.954	469.012	518.134	39.902	188.946	152466.352	2.680	3.462	6.425	3.107	289.183	6300.295
1670	26811.077	209485.767	1.059	402.575	709.132	46.353	272.058	172380.624	2.019	8.340	3.927	1.638	211.767	2956.812
1690	17409.641	285945.817	0.847	244.091	416.990	30.161	143.929	243103.547	1.845	5.385	2.419	1.348	223.182	2099.816
1710	24761.431	215638.874	1.855	757.689	978.136	51.513	409.825	180230.756	2.133	20.596	4.691	2.114	255.750	3383.178
1730	31881.983	170950.596	2.519	908.864	1426.687	68.096	468.934	145949.963	2.856	29.471	5.434	2.544	343.958	4847.608
1750	38933.453	223546.660	2.849	983.948	1333.783	102.114	612.647	179783.234	3.940	20.555	5.830	2.860	492.892	6019.622
1760	24326.073	178697.542	1.559	630.586	740.399	42.352	277.125	144755.510	2.865	6.949	3.427	2.673	378.283	4430.995
1780	31717.123	146975.980	2.595	1363.875	1298.029	55.265	567.671	126324.656	4.146	9.814	4.943	4.013	487.782	7480.600
1800	27714.264	142071.671	3.080	1286.134	1857.201	52.679	550.879	125099.313	4.273	20.399	4.706	4.816	438.807	6593.465
1820	33885.218	152627.590	2.143	1064.329	1340.694	36.368	328.024	127055.519	3.451	5.301	4.515	3.086	373.386	5954.700

1830	17100.625	124219.235	1.915	580.351	813.368	44.940	302.421	103790.794	2.079	11.550	2.974	1.282	245.151	2635.218
1850	21751.625	163404.691	2.579	957.049	1400.423	51.221	419.463	136013.478	2.308	17.642	4.352	2.032	310.292	3878.404
1870	37966.194	137627.804	2.185	812.020	909.187	57.633	320.793	131772.224	3.168	12.704	5.520	2.315	333.210	5568.666
1930	31028.510	182159.262	3.031	933.560	1226.170	113.063	462.172	146792.452	3.001	36.630	5.114	2.019	372.361	3111.750
1980	35269.297	73616.306	4.149	1778.633	1766.745	143.854	774.617	65173.656	4.220	20.501	4.305	3.040	515.558	2320.359
2020	61083.416	136045.567	4.853	1927.898	1997.115	71.607	758.587	115615.147	4.541	18.725	5.657	3.587	768.963	2294.219
2050	53200.011	112863.253	4.524	1783.404	1763.763	197.263	711.287	95583.736	5.094	22.872	5.771	2.662	801.329	1211.305
2070	53527.961	144929.003	4.740	1870.792	2754.715	222.486	961.269	118273.147	5.293	41.883	7.465	3.275	829.389	1875.895
2100	53963.918	111915.539	4.225	2127.192	2551.272	92.497	845.732	114091.763	6.001	14.924	6.187	4.808	761.051	5082.815
2260	60374.319	129057.659	3.136	626.882	663.325	43.843	295.583	101286.627	2.232	8.198	3.598	2.285	283.694	2394.160
2310	45709.933	147988.330	2.814	881.998	1346.584	76.325	424.555	120681.625	2.924	19.585	4.865	2.115	371.348	2616.634
2340	67064.290	131710.910	4.007	1270.100	1419.939	81.256	651.138	99579.592	3.407	23.878	6.550	2.835	465.264	3626.372
2380	34655.690	200388.823	2.447	1018.551	1018.890	60.738	406.385	161723.585	2.954	10.126	3.075	2.744	503.933	2214.347
2490	29759.971	298176.265	1.450	204.902	398.484	29.614	137.487	233586.033	1.629	2.724	3.469	0.711	290.684	423.763
2540	21457.453	429136.428	1.301	182.517	228.836	23.262	73.321	341700.143	1.182	1.774	2.773	0.824	237.349	634.953
2590	22237.031	65842.215	1.928	447.914	504.592	58.234	178.234	46750.338	1.800	3.530	0.968	1.555	364.864	339.703

Table 2: Continue/ Dingo 2 data set of major and trace elements.

Depth (m)	Co_ppm	Ni_ppm	Cu_ppm	Zn_ppm	Rb_ppm	Sr_ppm	Y_ppm	Zr_ppm	Nb_ppm	Mo_ppm	Cs_ppm	Ba_ppm	Hf_ppm	Ta_ppm	Pb_ppm	U_ppm
1400	42.197	40.409	33.618	76.312	1.561	65.998	23.670	0.155	0.309	0.595	0.182	49.561	0.022	0.040	121.733	1.087
1440	37.381	26.467	8.580	41.635	4.993	116.860	17.502	0.718	0.227	1.204	0.503	23.922	0.026	0.057	25.384	0.678
1460	23.674	9.665	12.104	40.349	4.184	66.104	11.398	0.180	0.329	0.242	0.518	22.966	0.019	0.043	12.625	0.632
1470	2.908	2.525	2.339	7.855	3.235	34.497	9.476	0.699	0.213	0.410	0.238	19.457	0.017	0.028	8.296	0.449
1500	19.253	11.038	15.261	39.160	7.131	40.664	19.592	0.609	0.215	0.181	0.589	64.343	0.025	0.028	9.810	0.845
1510	5.883	7.318	10.101	140.797	11.962	45.818	27.857	1.955	0.371	0.220	0.927	52.538	0.077	0.048	1.890	1.408
1530	9.534	4.625	4.018	39.093	11.573	74.881	22.711	1.490	0.277	0.164	0.602	84.207	0.119	0.036	4.845	2.127
1540	39.559	10.988	13.247	33.459	3.822	70.130	12.124	0.477	0.190	0.174	0.374	31.120	0.015	1.060	20.850	0.572
1550	5.601	2.433	2.699	10.127	1.729	65.694	8.201	0.315	0.344	0.204	0.144	13.176	0.013	0.351	9.521	0.358
1560	9.859	9.760	4.347	24.298	1.170	60.282	11.239	0.128	0.289	0.274	0.133	9.355	0.011	0.037	14.969	0.353
1570	3.098	2.723	2.813	8.789	3.202	88.424	11.316	0.899	0.287	0.170	0.242	10.209	0.025	1.747	6.234	0.493
1580	3.673	5.179	6.989	17.491	1.343	52.900	10.350	0.116	0.272	0.161	0.101	9.360	0.010	0.035	7.230	0.294
1590	2.800	1.715	1.611	10.159	1.187	148.502	8.580	0.344	0.233	0.191	0.108	6.055	0.013	0.030	24.925	0.358
1620	2.911	2.713	3.442	12.541	0.706	130.271	7.780	0.173	0.232	0.137	0.071	6.018	0.009	0.030	8.828	0.285
1640	12.224	3.489	1.543	8.866	1.090	195.167	11.604	0.277	0.210	0.124	0.165	17.934	0.008	0.031	7.539	0.383
1660	1.439	1.742	2.712	12.988	1.558	149.162	9.547	6.787	0.251	0.148	0.177	33.626	0.031	0.032	3.263	0.322
1670	1.400	1.305	0.887	4.106	1.742	171.643	8.768	0.299	0.241	0.143	0.161	30.069	0.011	0.061	3.808	0.357
1690	1.010	1.766	2.677	50.934	1.140	215.979	8.603	0.221	0.250	0.148	0.137	26.078	0.016	0.779	22.474	0.331
1710	14.966	1.873	0.941	10.178	3.458	164.804	9.148	0.232	0.280	0.166	0.287	22.704	0.022	0.036	5.146	0.537
1730	1.960	1.663	1.604	10.724	3.282	118.306	11.543	0.735	0.213	0.126	0.260	42.886	0.040	0.042	1.306	0.541
1750	4.853	2.571	2.332	9.010	4.580	173.304	16.811	0.605	0.271	0.161	0.239	28.490	0.019	0.035	6.548	0.587
1760	8.899	3.216	2.017	9.907	2.355	157.902	11.264	0.147	0.263	0.156	0.221	52.956	0.012	0.034	5.147	0.447
1780	11.675	3.335	3.627	23.863	4.498	124.555	13.441	0.253	0.238	0.141	0.355	54.442	0.013	0.031	4.047	0.504

1800	68.624	4.016	6.693	13.340	4.313	139.230	12.404	0.745	0.207	0.123	0.331	30.102	0.016	0.027	4.879	0.510
1820	2.860	2.087	2.086	11.243	2.756	138.308	10.916	0.371	0.282	0.167	0.198	39.170	0.012	0.037	3.417	0.422
1830	1.515	1.352	1.031	7.624	2.599	179.698	7.611	0.288	0.213	0.126	0.202	22.872	0.008	0.028	2.025	0.290
1850	1.696	1.649	1.426	12.125	3.266	618.688	8.499	0.271	0.248	0.147	0.182	65.029	0.009	0.032	5.376	0.471
1870	4.037	2.679	1.526	3.819	2.642	447.838	9.754	0.221	0.233	0.197	0.168	55.803	0.018	0.030	12.430	0.436
1930	3.704	1.648	2.349	11.965	4.661	678.225	10.409	0.257	0.230	0.136	0.288	97.629	0.014	0.030	2.802	0.552
1980	3.495	2.714	8.137	24.351	5.578	349.438	10.711	0.465	0.217	0.129	0.411	33.914	0.020	0.028	1.518	0.658
2020	8.698	3.383	149.721	64.459	5.708	945.276	11.799	1.007	0.308	0.182	0.522	104.594	0.026	0.040	4.320	1.042
2050	2.704	2.868	8.716	10.455	5.222	441.121	12.804	0.393	0.231	0.137	0.286	64.243	0.019	0.030	0.278	0.898
2070	2.824	2.818	8.852	10.353	6.256	464.928	15.082	0.856	0.224	0.133	0.445	57.843	0.036	0.032	0.574	1.037
2100	52.062	4.164	18.138	18.856	5.360	593.603	12.111	0.564	0.350	0.207	0.409	112.624	0.016	0.045	1.793	0.783
2260	11.426	1.864	2.899	13.933	2.747	1610.545	3.559	0.211	0.224	0.132	0.160	161.560	0.018	0.029	0.984	0.255
2310	9.201	1.504	1.763	8.115	3.142	692.101	7.305	0.562	0.252	0.149	0.268	54.674	0.012	0.033	1.897	0.407
2340	49.441	3.514	2.989	14.718	3.789	1147.703	6.438	0.732	0.293	0.174	0.202	95.452	0.017	0.038	10.971	0.518
2380	3.632	2.695	5.489	11.563	3.400	187.148	6.971	0.233	0.225	0.133	0.456	96.745	0.010	0.029	1.828	0.406
2490	7.795	0.716	0.644	8.335	0.785	595.478	4.165	0.210	0.238	0.141	0.134	32.968	0.009	0.031	0.659	0.827
2540	6.029	0.874	0.695	23.126	0.474	998.324	5.441	0.070	0.203	0.120	0.078	66.892	0.008	0.026	5.777	0.810
2590	1.923	1.012	9.790	33.169	1.077	147.930	3.191	0.181	0.247	0.146	0.231	28.489	0.009	0.032	10.980	0.284

Table 3: Dingo 2 REE data set.

Depth (m)	La_ppm	Ce_ppm	Pr_ppm	Nd_ppm	Sm_ppm	Eu_ppm	Gd_ppm	Tb_ppm	Dy_ppm	Ho_ppm	Er_ppm	Tm_ppm	Yb_ppm	Lu_ppm
1400	6.655	23.129	2.535	11.629	3.339	0.679	3.946	0.631	3.826	0.772	2.237	0.303	1.861	0.276
1440	7.643	22.330	2.499	10.968	2.691	0.594	3.054	0.492	3.114	0.612	1.793	0.244	1.489	0.237
1460	6.310	17.105	1.992	8.316	2.047	0.406	2.172	0.337	2.075	0.372	1.061	0.140	0.892	0.133
1470	6.481	17.553	2.105	8.508	1.921	0.351	1.916	0.296	1.683	0.323	0.871	0.118	0.641	0.095
1500	8.153	22.242	2.808	11.848	3.206	0.703	3.602	0.595	3.504	0.693	1.885	0.253	1.598	0.228
1510	11.950	34.027	4.520	20.733	5.773	1.234	6.541	0.971	5.747	1.014	2.600	0.335	1.946	0.304
1530	11.680	31.058	4.050	17.958	4.497	1.011	5.150	0.811	4.265	0.793	2.097	0.274	1.655	0.235
1540	6.500	17.487	2.060	8.694	2.208	0.467	2.308	0.372	2.193	0.425	1.193	0.167	0.993	0.142
1550	5.437	14.307	1.636	6.496	1.507	0.309	1.560	0.228	1.342	0.274	0.753	0.092	0.642	0.090
1560	12.751	28.488	2.804	10.576	2.134	0.390	2.151	0.320	1.990	0.381	1.104	0.143	0.933	0.135
1570	12.988	29.679	3.113	11.790	2.264	0.411	2.265	0.345	1.999	0.393	1.096	0.150	0.995	0.132
1580	10.129	23.852	2.499	9.761	1.970	0.371	1.960	0.322	1.872	0.359	1.024	0.134	0.841	0.115
1590	12.119	26.570	2.756	9.973	1.942	0.308	1.844	0.266	1.530	0.296	0.833	0.105	0.688	0.100
1620	10.874	23.936	2.483	9.150	1.724	0.298	1.540	0.244	1.390	0.276	0.707	0.099	0.600	0.086
1640	16.478	35.064	3.625	13.353	2.466	0.429	2.382	0.351	2.030	0.398	1.151	0.157	0.950	0.130
1660	12.853	27.240	3.003	10.752	1.989	0.375	1.950	0.328	1.700	0.353	0.937	0.158	0.772	0.133
1670	12.886	26.298	2.860	10.381	1.892	0.341	1.761	0.259	1.500	0.292	0.827	0.109	0.715	0.103
1690	12.854	26.691	2.872	10.162	1.900	0.304	1.878	0.270	1.498	0.286	0.827	0.111	0.689	0.094
1710	11.506	24.363	2.735	10.181	2.051	0.371	1.922	0.293	1.635	0.295	0.851	0.109	0.720	0.103
1730	14.410	29.892	3.351	12.544	2.540	0.465	2.481	0.358	2.005	0.397	1.049	0.137	0.865	0.127
1750	19.648	40.560	4.657	17.916	3.646	0.722	3.625	0.529	2.963	0.576	1.538	0.208	1.263	0.176

1760	14.552	30.680	3.427	12.669	2.524	0.467	2.402	0.358	2.033	0.379	1.001	0.135	0.860	0.118
1780	12.089	27.813	3.258	13.004	2.779	0.582	2.977	0.438	2.408	0.443	1.256	0.162	1.021	0.143
1800	15.938	34.390	3.883	14.603	2.920	0.552	2.740	0.406	2.355	0.426	1.174	0.153	1.015	0.141
1820	13.519	28.819	3.175	11.968	2.341	0.447	2.329	0.343	1.989	0.376	1.052	0.146	0.855	0.117
1830	10.416	21.500	2.376	8.912	1.708	0.317	1.669	0.255	1.313	0.247	0.726	0.101	0.587	0.086
1850	12.062	23.998	2.709	10.009	1.884	0.366	1.732	0.259	1.499	0.290	0.781	0.110	0.659	0.090
1870	11.164	24.156	2.739	10.317	2.082	0.394	2.036	0.301	1.734	0.339	0.931	0.125	0.749	0.109
1930	12.281	25.726	2.962	11.294	2.329	0.481	2.315	0.340	2.006	0.364	0.960	0.123	0.789	0.113
1980	6.705	15.699	2.067	9.005	2.297	0.509	2.631	0.380	2.091	0.383	1.030	0.126	0.810	0.105
2020	8.207	18.989	2.387	10.155	2.561	0.544	2.741	0.393	2.109	0.405	1.039	0.131	0.812	0.106
2050	6.796	15.352	2.286	10.328	2.770	0.626	3.158	0.451	2.381	0.439	1.096	0.144	0.916	0.133
2070	9.461	20.304	2.871	12.613	3.355	0.724	3.615	0.534	2.870	0.525	1.319	0.169	1.061	0.169
2100	8.135	19.053	2.416	10.073	2.711	0.546	2.788	0.418	2.299	0.441	1.097	0.146	0.933	0.135
2260	2.965	7.229	0.939	3.657	0.889	0.179	0.815	0.124	0.679	0.119	0.328	0.038	0.218	0.036
2310	7.049	15.682	1.861	7.568	1.678	0.346	1.685	0.287	1.375	0.256	0.677	0.093	0.532	0.079
2340	4.310	11.153	1.550	6.870	1.563	0.340	1.596	0.246	1.292	0.221	0.577	0.081	0.454	0.064
2380	6.763	13.669	1.609	6.554	1.454	0.316	1.515	0.229	1.316	0.234	0.615	0.077	0.459	0.072
2490	5.798	10.424	1.263	4.568	0.887	0.195	0.921	0.142	0.780	0.137	0.367	0.049	0.274	0.039
2540	8.805	16.353	1.809	6.680	1.259	0.262	1.199	0.171	0.962	0.163	0.433	0.060	0.371	0.049
2590	1.842	3.723	0.818	3.572	0.938	0.238	0.901	0.125	0.657	0.101	0.293	0.036	0.237	0.032

Table 4: Alice 1 data set of major and trace elements.

Depth (m)	Mg_ppm	Ca_ppm	Li_ppm	Al_ppm	Si_ppm	P_ppm	K_ppm	Ca_ppm	Sc_ppm	Ti_ppm	V_ppm	Cr_ppm	Mn_ppm	Fe_ppm
872	122769.501	268866.148	0.000	815.042	2147.128	2449.574	271.958	216425.681	1.253	12.814	2.466	3.772	3643.546	3534.095
917	91405.765	169969.234	0.145	898.511	1544.001	929.572	524.703	169663.828	1.700	19.838	6.619	5.020	1396.370	4178.417
927	103116.312	176669.189	0.142	406.490	822.204	353.515	219.848	176890.014	0.833	8.337	7.444	3.459	1338.360	5998.499
954	104221.558	184366.102	0.137	450.733	961.721	326.007	276.104	175262.641	1.137	12.765	4.806	3.287	853.518	5203.308
1021	15548.055	142898.874	0.181	348.203	508.465	161.826	189.028	133432.970	1.036	4.160	3.136	6.066	301.629	2248.677
1045	58515.606	118817.666	2.696	1413.372	1915.391	340.842	853.359	115893.068	5.454	24.361	7.744	4.836	678.430	7479.174
1070	89831.647	182133.851	2.398	2146.805	1768.691	664.364	780.374	181587.408	4.801	1.982	10.940	21.126	1889.925	12357.127
1079	84237.444	164172.143	1.250	852.018	729.590	236.616	406.802	150778.602	4.658	3.079	8.408	5.319	1010.669	9945.243
1088	72792.152	137637.224	0.815	901.609	647.470	197.051	321.598	132265.394	4.274	0.657	7.948	3.987	734.324	8496.765
1097	99253.508	185700.584	1.619	1791.374	1172.341	313.007	599.258	183960.658	4.506	2.277	9.053	12.659	1018.534	13090.650
1106	99084.256	174949.957	0.237	399.682	375.851	164.651	218.403	178138.115	2.422	0.909	4.549	3.051	943.381	13311.433
1116	110745.858	198947.435	0.399	598.853	1082.901	181.823	328.780	192336.710	1.895	10.277	6.503	3.628	737.219	9246.970
1152	92233.885	165364.677	0.167	238.432	250.261	139.042	134.735	166048.606	1.485	1.926	5.350	3.959	547.665	5934.553
1180	52030.277	147541.522	0.398	788.820	1007.757	234.596	375.590	144265.753	2.475	151.168	5.654	5.508	385.982	4540.536
1189	57744.748	191153.726	0.190	262.945	281.920	82.357	130.904	194191.641	2.113	3.475	4.564	4.782	391.405	5150.166
1198	72942.756	179633.908	0.154	244.409	287.702	157.494	132.213	169199.874	2.604	1.532	6.958	4.282	416.106	5247.901
1207	60608.257	177782.563	0.880	916.404	2207.052	228.283	537.942	175071.315	3.221	27.498	8.504	8.551	412.795	5580.679
1225	29707.191	176806.842	0.169	309.311	302.089	59.504	136.456	169150.595	1.529	1.151	3.886	1.943	247.312	2604.926
1253	12797.819	314261.117	0.148	117.290	188.598	58.649	70.692	294966.061	1.389	2.963	1.129	2.530	354.461	2044.194

1280	24219.586	243105.606	0.343	331.575	462.377	22.954	123.714	231912.473	1.340	1.039	2.674	5.343	300.051	3363.861
1298	63669.649	134849.747	2.525	1054.830	1519.997	95.807	555.347	128169.833	4.813	30.693	8.316	4.246	352.519	7990.337
1344	31339.079	130626.143	2.009	1687.611	2632.987	151.813	755.698	127320.286	2.811	23.629	5.839	5.817	333.268	3988.092
1362	19484.695	117780.786	0.344	397.344	508.493	37.693	219.416	115008.485	1.598	4.907	2.722	2.176	285.614	2581.266
1372	14411.350	157197.945	0.376	380.864	472.017	88.940	175.287	140755.048	1.207	2.084	2.441	3.385	236.849	2043.811
1381	34947.478	204915.055	1.836	860.615	1546.687	64.461	417.099	189095.426	3.578	23.942	5.984	3.795	349.031	5346.848
1390	21218.633	186048.587	0.865	542.290	906.744	46.545	283.712	177647.473	2.420	10.582	3.643	2.286	294.099	3341.894
1399	21268.858	169261.769	1.442	717.097	1393.185	49.953	432.134	162687.240	1.796	20.958	4.233	2.486	264.192	3464.044
1408	37284.462	173869.610	2.079	1257.621	1884.438	84.014	611.722	163953.748	2.987	22.254	5.102	4.441	355.259	5058.639
1417	33548.753	196487.006	0.508	605.636	1003.675	105.297	308.055	196442.474	1.905	6.170	4.376	2.901	335.032	3343.970
1426	28280.235	203561.793	0.971	856.790	1349.005	60.348	375.665	196285.110	2.578	23.860	3.084	7.359	322.331	3567.283
1515	31774.227	105454.568	2.600	1352.635	2333.124	257.115	655.457	104853.159	2.184	24.461	4.868	3.688	271.138	1782.628
1545	19627.862	182921.263	0.620	387.021	472.884	46.716	166.765	172971.684	1.334	1.412	1.708	2.891	243.423	1187.481
1554	15876.751	213215.113	0.378	393.698	520.054	48.005	143.570	203258.424	0.991	2.212	1.669	2.430	239.751	1197.209
1570	30267.744	211175.881	0.412	418.939	517.673	17.818	154.318	214193.808	1.473	3.170	1.597	3.535	263.815	1929.036
1600	63461.310	130610.695	4.148	1161.526	2104.139	130.709	565.593	131915.205	3.105	25.186	6.676	3.054	459.012	2592.782
1628	77417.080	162504.790	2.096	725.472	1373.717	54.805	411.412	156219.683	2.104	21.477	8.077	7.232	498.496	2368.496
1719	75119.268	148940.401	2.853	1104.306	1900.226	105.972	496.047	148740.080	4.207	34.845	6.790	4.097	516.863	2979.907
1756	82194.014	150386.692	2.960	698.832	1599.201	148.974	369.307	158127.153	2.256	17.694	6.552	4.616	423.775	1943.796
1774	78921.066	153707.123	1.460	710.568	761.540	341.203	362.476	160598.297	3.310	1.017	6.558	19.176	568.436	3325.109
1820	87096.501	163489.949	3.931	566.615	1023.126	47.000	270.588	153254.527	1.367	13.743	5.469	3.805	223.728	3119.610
1856	88581.872	173149.559	0.815	184.319	379.931	34.816	100.534	176539.939	0.871	2.179	4.881	3.298	195.045	3550.226
1902	57378.555	108773.677	4.786	1637.183	2156.867	281.442	931.424	118071.723	4.142	35.650	9.074	4.477	435.014	4765.139
1939	95619.972	186651.738	2.020	437.212	601.332	55.845	220.313	187847.430	2.076	6.288	5.867	5.075	305.438	3115.086
1960	33072.630	100980.596	2.019	1678.579	1867.624	80.219	344.186	99919.396	2.186	9.971	4.998	5.432	261.316	1624.043
1987	66852.908	125949.540	6.983	2471.474	3236.067	1122.250	1098.918	129691.484	5.309	37.001	10.874	19.963	848.239	5694.102
1996	82572.767	149607.753	3.597	1407.093	2785.241	224.396	778.098	148702.472	2.367	38.644	6.530	6.521	1006.204	7348.010

Table 4: Continue/ Alice 1 data set of major and trace elements.

Depth (m)	Co_ppm	Ni_ppm	Cu_ppm	Zn_ppm	Rb_ppm	Sr_ppm	Y_ppm	Zr_ppm	Nb_ppm	Mo_ppm	Cs_ppm	Ba_ppm	Hf_ppm	Ta_ppm	Pb_ppm	U_ppm
872	3.326	4.255	8.915	53.143	1.349	46.218	26.804	1.299	0.229	0.205	0.147	76.625	0.054	0.102	29.148	3.963
917	3.176	3.697	11.299	51.624	2.563	60.910	15.683	1.326	0.148	0.133	0.164	9.988	0.050	0.052	82.876	0.756
927	2.895	2.732	4.290	73.400	1.331	34.608	10.320	0.635	0.145	0.224	0.089	49.268	0.026	0.038	305.412	0.926
954	1.862	2.314	2.312	26.416	1.308	31.200	8.623	0.837	0.140	0.126	0.086	19.845	0.030	0.025	65.828	0.805
1021	1.375	1.911	2.110	57.352	1.029	86.179	7.668	0.155	0.185	0.177	0.114	31.640	0.014	0.033	146.974	0.350
1045	8.416	6.574	6.481	41.464	5.563	77.771	16.908	0.657	0.165	1.457	0.283	125.287	0.031	0.040	121.689	0.693
1070	5.636	7.178	8.538	497.572	5.426	123.177	25.591	0.204	0.218	0.388	0.430	530.444	0.022	0.039	196.746	2.563
1079	3.039	2.406	4.838	161.671	3.005	67.230	18.946	0.126	0.174	0.500	0.270	28.847	0.020	0.031	235.874	0.696
1088	4.297	2.512	2.589	24.867	2.513	58.032	15.858	0.023	0.203	0.182	0.125	219.583	0.010	0.036	10.484	0.511
1097	4.402	6.162	8.046	852.167	3.941	102.367	18.009	0.155	0.193	0.456	0.172	298.401	0.013	0.035	715.278	0.880
1106	2.219	3.172	1.953	53.007	1.603	46.960	12.117	0.036	0.243	0.218	0.150	18.121	0.012	0.044	19.649	0.368

1116	2.174	2.869	3.362	33.460	1.920	51.325	10.204	0.397	0.219	0.196	0.155	74.662	0.013	0.039	427.165	0.403
1152	1.341	1.488	1.879	32.766	1.071	43.857	8.343	0.052	0.172	0.583	0.106	18.822	0.009	0.031	26.510	0.280
1180	2.744	3.098	6.189	12.597	2.325	77.142	11.262	2.504	0.203	0.250	0.177	48.248	0.021	0.036	19.064	2.463
1189	1.364	1.848	1.660	1764.799	0.879	119.350	8.695	0.099	0.195	0.175	0.120	18.476	0.024	0.054	319.238	0.242
1198	1.486	1.560	1.412	58.044	1.086	84.128	11.003	0.071	0.158	0.165	0.097	57.952	0.024	0.032	76.779	0.276
1207	2.294	2.885	2.056	26.838	3.524	109.292	14.055	1.654	0.188	0.220	0.184	164.939	0.063	0.046	20.934	0.444
1225	1.808	1.601	0.915	16.065	1.394	88.127	6.709	0.036	0.174	0.156	0.107	2.300	0.011	0.031	4.956	0.265
1253	0.631	0.703	0.327	22.158	0.360	261.240	14.822	0.046	0.152	0.137	0.094	7.000	0.009	0.027	6.247	0.123
1280	1.243	1.497	0.622	633.189	0.832	172.366	7.125	0.102	0.183	0.164	0.112	37.428	0.009	0.033	61.659	0.235
1298	5.001	3.254	1.932	6.652	4.024	123.065	10.395	0.562	0.168	0.150	0.237	27.441	0.030	0.108	7.886	0.424
1344	2.862	2.827	2.095	235.619	4.274	99.252	8.783	1.675	0.179	0.160	0.256	36.127	0.054	0.032	76.534	0.798
1362	1.610	1.224	0.688	2.321	1.547	202.429	8.582	0.097	0.156	0.140	0.096	141.993	0.008	0.028	2.199	0.271
1372	1.301	1.430	0.786	2166.404	1.208	132.657	6.299	0.195	1.041	0.145	0.100	22.723	0.014	0.029	280.924	0.341
1381	4.210	3.450	1.604	9.471	2.884	200.025	10.544	0.685	0.163	0.146	0.160	64.784	0.022	0.029	15.641	0.443
1390	2.002	1.430	0.857	6.580	2.301	133.096	7.907	0.327	0.185	0.166	0.141	10.742	0.012	0.033	4.077	0.193
1399	1.724	1.550	0.664	1.776	2.546	356.507	7.643	0.409	0.177	0.159	0.125	49.133	0.024	0.032	6.592	0.390
1408	2.807	2.883	1.646	29.295	3.841	196.092	12.665	0.727	0.148	0.133	0.216	53.888	0.041	0.027	4.780	0.553
1417	1.355	1.173	0.628	17.579	1.633	431.551	8.711	0.551	0.198	0.178	0.122	82.381	0.027	0.036	6.719	0.367
1426	2.973	2.784	7.633	1435.917	2.404	234.562	9.611	0.523	0.199	0.179	0.147	68.743	0.016	0.036	51.999	0.372
1515	1.547	1.963	1.772	52.975	3.675	938.250	8.081	1.501	0.175	0.157	0.229	101.767	0.040	0.031	7.610	0.660
1545	1.122	1.074	0.604	106.118	1.031	346.814	7.402	0.086	0.160	0.144	0.098	23.793	0.008	0.029	3.290	0.197
1554	0.912	0.766	0.370	38.867	0.900	227.593	6.739	0.280	0.143	0.128	0.088	8.177	0.014	0.026	7.197	0.273
1570	1.520	1.200	1.097	127.668	1.131	415.564	7.021	0.296	0.150	0.135	0.093	34.420	0.019	0.027	5.404	0.254
1600	1.511	1.601	0.581	26.273	3.628	2953.551	8.306	0.622	0.170	0.135	0.220	329.488	0.042	0.100	0.681	0.461
1628	1.870	1.217	8.328	4.866	2.527	642.746	11.427	0.414	0.161	0.357	0.159	43.300	0.018	0.029	0.634	0.915
1719	3.399	1.845	1.429	4.027	3.516	996.014	7.628	0.656	0.176	0.158	0.175	159.941	0.022	0.032	1.814	0.342
1756	1.612	2.576	2.305	223.299	2.478	1611.350	5.840	0.294	0.190	0.171	0.152	114.353	0.017	0.034	34.983	0.587
1774	3.420	2.389	6.581	210.080	2.644	1070.171	11.578	0.145	0.212	0.219	0.217	121.856	0.014	0.038	12.467	0.498
1820	1.616	1.708	1.254	130.065	2.350	2093.911	3.468	0.191	0.150	1.019	0.162	78.431	0.016	0.078	3.230	0.355
1856	0.960	1.163	0.869	14.334	0.782	1086.873	3.750	0.047	0.157	1.692	0.096	141.525	0.008	0.028	6.512	0.203
1902	2.691	7.412	0.998	34.767	4.834	1965.912	10.416	0.607	0.190	0.170	0.197	207.831	0.021	0.034	2.605	0.373
1939	1.816	1.476	1.103	27.253	2.091	4524.954	5.122	0.094	0.141	0.284	0.123	393.836	0.031	0.105	5.898	0.270
1960	2.884	2.823	2.295	10.778	2.210	647.035	4.820	0.433	0.155	0.139	0.101	44.799	0.017	0.028	5.200	0.318
1987	6.290	6.465	2.842	43.535	6.744	447.560	14.917	0.635	0.143	0.633	0.482	48.737	0.035	0.026	4.892	0.430
1996	3.275	3.138	1.408	11.063	4.936	156.574	5.202	0.735	0.174	0.281	0.375	26.802	0.024	0.031	4.915	0.426

Table 5: Alice 1 REE data set.

Depth (m)	La_ppm	Ce_ppm	Pr_ppm	Nd_ppm	Sm_ppm	Eu_ppm	Gd_ppm	Tb_ppm	Dy_ppm	Ho_ppm	Er_ppm	Tm_ppm	Yb_ppm	Lu_ppm
872	12.265	38.898	5.323	23.659	5.467	1.128	5.689	0.847	4.724	0.931	2.494	0.319	1.831	0.256
917	8.978	27.568	3.235	14.672	3.450	0.622	3.407	0.518	2.786	0.551	1.503	0.202	1.178	0.177
927	6.703	18.830	2.011	8.076	1.862	0.361	1.906	0.316	1.710	0.349	0.972	0.133	0.760	0.122
954	7.989	20.652	2.219	8.887	1.807	0.338	1.854	0.268	1.552	0.309	0.805	0.107	0.690	0.104

1021	8.935	20.430	2.164	8.309	1.632	0.341	1.675	0.250	1.400	0.260	0.743	0.104	0.623	0.103
1045	9.962	25.997	3.186	14.048	3.780	0.726	3.729	0.602	3.266	0.632	1.698	0.214	1.326	0.167
1070	9.532	27.246	3.616	16.763	4.840	1.141	5.695	0.929	5.027	0.957	2.483	0.319	2.024	0.282
1079	9.352	24.106	2.993	12.838	3.607	0.774	4.064	0.660	3.696	0.700	1.863	0.236	1.471	0.200
1088	8.840	23.291	2.754	11.891	3.180	0.686	3.337	0.533	3.112	0.577	1.546	0.207	1.248	0.181
1097	10.152	25.574	3.093	12.576	3.295	0.698	3.259	0.553	3.280	0.639	1.849	0.248	1.607	0.214
1106	9.736	23.865	2.518	10.148	2.214	0.485	2.378	0.410	2.181	0.446	1.211	0.144	0.919	0.146
1116	8.613	22.429	2.292	9.199	1.995	0.412	2.116	0.347	1.899	0.360	0.965	0.122	0.782	0.115
1152	9.001	20.700	2.166	8.351	1.698	0.350	1.695	0.261	1.499	0.280	0.772	0.091	0.584	0.081
1180	13.019	29.808	3.294	12.730	2.638	0.511	2.527	0.382	2.104	0.385	1.070	0.140	0.898	0.120
1189	11.373	24.882	2.627	9.837	1.946	0.354	1.873	0.277	1.539	0.324	0.809	0.122	0.684	0.102
1198	12.181	27.522	3.055	11.615	2.432	0.484	2.422	0.362	1.994	0.387	1.031	0.135	0.844	0.116
1207	16.064	36.708	3.999	15.066	3.125	0.634	2.980	0.470	2.591	0.512	1.409	0.177	1.148	0.162
1225	8.657	18.559	2.039	7.631	1.469	0.284	1.380	0.228	1.212	0.239	0.646	0.092	0.564	0.078
1253	17.353	40.467	3.697	13.384	2.648	0.531	2.770	0.426	2.489	0.500	1.403	0.199	1.247	0.182
1280	9.320	20.044	2.149	7.674	1.547	0.288	1.450	0.217	1.263	0.239	0.683	0.092	0.574	0.092
1298	11.548	25.729	3.000	11.332	2.296	0.479	2.174	0.352	1.993	0.375	1.085	0.151	0.864	0.115
1344	11.427	26.883	3.034	11.692	2.275	0.454	2.083	0.320	1.766	0.312	0.880	0.109	0.669	0.114
1362	11.006	22.861	2.620	9.900	2.068	0.398	1.871	0.278	1.496	0.302	0.800	0.103	0.627	0.091
1372	8.723	17.926	2.016	7.434	1.497	0.290	1.330	0.206	1.148	0.220	0.570	0.076	0.438	0.063
1381	14.505	30.195	3.385	12.372	2.469	0.460	2.336	0.344	1.874	0.354	0.950	0.129	0.839	0.113
1390	11.542	24.201	2.682	9.507	1.876	0.349	1.811	0.255	1.421	0.270	0.736	0.098	0.606	0.089
1399	10.960	21.753	2.382	8.625	1.651	0.319	1.632	0.240	1.346	0.262	0.724	0.093	0.570	0.078
1408	15.979	33.834	3.940	14.938	3.058	0.579	2.876	0.422	2.351	0.447	1.183	0.159	0.963	0.141
1417	11.667	24.471	2.733	9.815	2.019	0.367	1.899	0.291	1.573	0.286	0.841	0.097	0.651	0.088
1426	12.408	27.478	3.131	11.847	2.367	0.451	2.226	0.330	1.804	0.360	0.927	0.130	0.764	0.111
1515	9.207	19.851	2.512	10.273	2.142	0.453	2.180	0.322	1.569	0.293	0.761	0.094	0.539	0.081
1545	9.773	19.228	2.247	8.537	1.653	0.337	1.620	0.248	1.305	0.254	0.643	0.082	0.510	0.071
1554	9.930	19.486	2.210	8.051	1.575	0.304	1.541	0.217	1.209	0.216	0.581	0.077	0.471	0.066
1570	10.147	20.380	2.278	8.207	1.588	0.284	1.462	0.230	1.230	0.245	0.649	0.089	0.528	0.070
1600	6.268	14.457	1.796	7.375	1.835	0.400	1.940	0.274	1.540	0.290	0.714	0.094	0.604	0.085
1628	9.251	19.623	2.450	9.743	2.171	0.483	2.487	0.347	1.949	0.378	0.981	0.129	0.742	0.099
1719	5.217	12.164	1.654	7.037	1.817	0.437	1.831	0.285	1.495	0.277	0.776	0.096	0.565	0.077
1756	4.607	10.794	1.381	5.711	1.376	0.310	1.447	0.208	1.172	0.198	0.514	0.069	0.386	0.050
1774	6.316	16.822	2.415	11.358	3.050	0.611	3.001	0.454	2.254	0.406	1.058	0.123	0.768	0.116
1820	3.324	7.483	0.898	3.554	0.815	0.152	0.750	0.127	0.661	0.123	0.369	0.040	0.215	0.033
1856	3.866	8.146	0.988	3.825	0.818	0.175	0.861	0.121	0.690	0.130	0.317	0.041	0.272	0.035
1902	6.323	16.566	2.228	9.699	2.579	0.581	2.737	0.414	2.111	0.375	0.974	0.121	0.716	0.100
1939	4.055	10.002	1.297	5.304	1.203	0.285	1.221	0.195	1.003	0.174	0.451	0.054	0.348	0.047
1960	3.734	10.237	1.272	5.060	1.231	0.243	1.067	0.165	0.889	0.164	0.448	0.062	0.408	0.050
1987	11.699	29.847	3.887	16.919	4.112	0.868	4.071	0.571	3.009	0.535	1.310	0.159	0.940	0.138
1996	5.638	11.115	1.498	5.732	1.311	0.246	1.201	0.191	0.967	0.174	0.455	0.057	0.308	0.044

Table 5: Dingo 2 and Alice 1 Strontium isotope data set.

Hole_ID	Depth (m)	Mean (After)	2se
Dingo 2	1400	.710493	.000003
Dingo 2	1440	.711500	.000003
Dingo 2	1460	.711724	.000003
Dingo 2	1470	.713092	.000005
Dingo 2	1500	.714667	.000004
Dingo 2	1510	.717502	.000004
Dingo 2	1530	.713893	.000003
Dingo 2	1540	.711307	.000003
Dingo 2	1550	.710940	.000003
Dingo 2	1560	.710811	.000004
Dingo 2	1570	.711820	.000003
Dingo 2	1580	.710715	.000004
Dingo 2	1590	.709857	.000003
Dingo 2	1620	.709655	.000003
Dingo 2	1640	.709674	.000004
Dingo 2	1660	.709899	.000003
Dingo 2	1670	.709853	.000004
Dingo 2	1690	.709662	.000003
Dingo 2	1710	.710206	.000003
Dingo 2	1730	.710736	.000004
Dingo 2	1750	.710982	.000003
Dingo 2	1760	.710565	.000003
Dingo 2	1780	.711383	.000004
Dingo 2	1800	.711480	.000003
Dingo 2	1820	.710632	.000003
Dingo 2	1830	.710273	.000003
Dingo 2	1850	.709815	.000004
Dingo 2	1870	.710233	.000003
Dingo 2	1930	.710258	.000003
Dingo 2	1980	.710554	.000004
Dingo 2	2020	.710172	.000003
Dingo 2	2050	.710426	.000003
Dingo 2	2070	.710447	.000003
Dingo 2	2100	.710317	.000004
Dingo 2	2260	.709259	.000004
Dingo 2	2310	.709543	.000003
Dingo 2	2340	.709568	.000004
Dingo 2	2380	.710400	.000003
Dingo 2	2490	.709566	.000003
Dingo 2	2540	.709325	.000003
Dingo 2	2590	.710063	.000004

Hole_ID	Depth_from	87/86 Sr	2se
Alice 1	872	.712020	.000004
Alice 1	917	.710640	.000004
Alice 1	927	.710219	.000004
Alice 1	954	.710778	.000004
Alice 1	1021	.709825	.000004
Alice 1	1045	.713502	.000003
Alice 1	1070	.712276	.000005
Alice 1	1079	.711959	.000004
Alice 1	1088	.710940	.000003
Alice 1	1097	.711510	.000003
Alice 1	1106	.710309	.000003
Alice 1	1116	.710813	.000003
Alice 1	1152	.710130	.000003
Alice 1	1180	.710781	.000003
Alice 1	1189	.709604	.000004
Alice 1	1207	.710383	.000003
Alice 1	1225	.709841	.000003
Alice 1	1253	.709370	.000004
Alice 1	1280	.709661	.000003
Alice 1	1298	.711024	.000004
Alice 1	1344	.711042	.000004
Alice 1	1362	.710286	.000003
Alice 1	1372	.709953	.000004
Alice 1	1381	.710483	.000003
Alice 1	1390	.709966	.000003
Alice 1	1399	.709819	.000003
Alice 1	1408	.710129	.000003
Alice 1	1417	.709763	.000003
Alice 1	1426	.710044	.000004
Alice 1	1515	.709931	.000003
Alice 1	1545	.709635	.000003
Alice 1	1554	.709632	.000003
Alice 1	1570	.709607	.000004
Alice 1	1600	.709479	.000003
Alice 1	1628	.709665	.000004
Alice 1	1719	.709562	.000003
Alice 1	1756	.709353	.000002
Alice 1	1774	.709532	.000003
Alice 1	1820	.709221	.000003
Alice 1	1856	.709283	.000004
Alice 1	1902	.709350	.000003
Alice 1	1939	.709180	.000004
Alice 1	1960	.709291	.000003
Alice 1	1987	.709864	.000003
Alice 1	1996	.710994	.000005